รายงานวิจัยฉบับสมบูรณ์

โครงการ แบบจำลองทางพลวัตเชิงโมเลกุลที่รวมระเบียบวิธี แอบ อินิชิโอ กลศาสตร์ควอนตัมและกลศาสตร์โมเลกุลของไอออนโลหะขนาดใหญ่และประจุสูงในน้ำ

โดย ผู้ช่วยศาสตราจารย์ ดร.ชินพงษ์ กฤตยากรนุพงศ์

มีนาคม 2554

สัญญาเลขที่ TRG5280015

รายงานวิจัยฉบับสมบูรณ์

โครงการ แบบจำลองทางพลวัตเชิงโมเลกุลที่รวมระเบียบวิธี แอบ อินิชิโอ กลศาสตร์ควอนตัมและกลศาสตร์โมเลกุลของไอออนโลหะขนาดใหญ่และประจุสูงในน้ำ

ผู้วิจัย
ผู้ช่วยศาสตราจารย์ ดร.ชินพงษ์ กฤตยากรนุพงศ์

สังกัด
ภาควิชาเคมี คณะวิทยาศาสตร์
มหาวิทยาลัยเทคโนโลยีพระจอมเกล้าธนบุรี

สนับสนุนโดยสำนักงานกองทุนสนับสนุนการวิจัย

กิตติกรรมประกาศ

ผู้วิจัยขอขอบพระคุณอาจารย์ที่ปรึกษา ศาสตราจารย์ ดร.สุพจน์ หารหนองบัว และ Prof. Dr. Bernd Michael Rode ที่ให้คำปรึกษาอันทรงคุณค่า รวมถึงแนะนำการเป็นการนักจัย โครงการนี้ไม่อาจสำเร็จลงได้หากปราศจากอาจารย์ทั้งสองท่าน

ผู้วิจัยขอขอบคุณ ผู้ช่วยศาสตราจารย์ ดร.วิวัฒน์ วชิรวงศ์กวิน อาจารย์ประจำภาควิชาเคมี คณะวิทยาศาสตร์ จุฬาลงกรณ์มหาวิทยาลัย ที่ให้ความร่วมมือในงานวิจัยภายใต้โครงการนี้เป็นอย่างดี

สุดท้ายนี้ ผู้วิจัยขอขอบพระคุณสำนักกองทุนสนับสนุนการวิจัย ซึ่งเป็นแหล่งทุนภายนอกที่ให้การสนับสนุนงานวิจัยของผู้วิจัยเป็นอย่างดีเสมอมา

รหัสโครงการ: TRG5280015

ชื่อโครงการ: แบบจำลองทางพลวัตเชิงโมเลกุลที่รวมระเบียบวิธี แอบ อินิชิโอ กลศาสตร์ควอนตัมและกลศาสตร์โมเลกุลของไอออนโลหะขนาดใหญ่และประจุสูงในน้ำ

ชื่อนักวิจัย: ผู้ช่วยศาสตราจารย์ ดร.ชินพงษ์ กฤตยากรนุพงศ์
ภาควิชาเคมี คณะวิทยาศาสตร์ มหาวิทยาลัยเทคโนโลยีพระจอมเกล้าธนบุรี

E-mail Address: chinapong.kri@kmutt.ac.th

ระยะเวลาโครงการ: 2 ปี

บทคัดย่อ:

ในงานวิจัยนี้ ทำการศึกษาสมบัติทางโครงสร้างและพลศาสตร์ของ V^{3+} HS^- HCl และ HSO_4^- ในน้ำ คำนวณโดยแบบจำลองพลวัตเชิงโมเลกุลที่รวมกลศาสตร์ควอนตัมและกลศาสตร์โมเลกุลและแบบจำลองพลวัตเชิงโมเลกุลกลศาสตร์ควอนตัมในสนามประจุ สมบัติทางโครงสร้างแสดงในเทอมการกระจายในแนวรัศมีและเลขโคออร์ดิเนชันของชั้นซอลเวชัน ซึ่งค่าที่ได้จากการคำนวณสอดคล้องกับผลการทดลองเป็นอย่างดี นอกจากนี้ การจัดเรียงตัวของโมเลกุลน้ำรอบตัวถูกละลายสามารถอธิบายโดยค่าการกระจายของมุมต่างๆ สำหรับสมบัติทางพลศาสตร์วิเคราะห์โดยค่าระยะเวลาเฉลี่ยของตัวทำละลายในชั้นซอลเวชันและค่าสเปคตรัมการสั่นเพื่อเปรียบเทียบกับผลการทดลอง สุดท้าย เวลาเฉลี่ยการเกิดพันธะไฮโดรเจนถูกใช้สำหรับอธิบายความเสถียรของพันธะไฮโดรเจนในแต่ละระบบ

คำหลัก: V^{3+} HS^- HCl HSO_4^- แบบจำลองพลวัตเชิงโมเลกุล

Project Code: TRG5280015

Project Title: *Ab initio* quantum mechanical/molecular mechanics molecular dynamics simulations of some large and highly charged metal ions in aqueous solution

Investigator: Assistant Professor Dr. Chinapong Kritayakornupong

E-mail Address: chinapong.kri@kmutt.ac.th

Project period: 2 years

Abstract:

The hybrid *ab initio* quantum mechanical/molecular mechanical (QM/MM) and *ab initio* quantum mechanical charge field (QMCF) molecular dynamics simulations were performed to study structure and dynamics of the V^{3+}, HS^-, HCl, and HSO_4^-. Hydration structures were determined in terms of radial distribution functions and coordination numbers, which are in good agreement with the experiments. In addition, tilt- and θ-angle distributions were also elucidated for describing the geometrical arrangement of water molecules around the solute species. For the dynamical information, the mobility of ligands in the solvation shell for each system was estimated by means of the mean residence times. The vibrational spectra were analyzed to compare with the experimental IR results. Finally, the hydrogen bond life times were determined to characterize a very different stability of H-bonds in each system.

Keywords: V^{3+}, HS^-, HCl, HSO_4^-, Molecular dynamics simulation

1. บทนำ

นักเคมีและนักชีวเคมีให้ความสนใจกับพฤติกรรมของไอออนรวมถึงสารประกอบไอออนเมื่ออยู่ในสารละลาย เนื่องกระบวนการทางเคมีและชีวเคมีมักเกิดในระบบสารละลายไอออนต่างๆ โดยทั่วไปสมบัติทางโครงสร้างและพลศาสตร์ของไอออนสามารถศึกษาโดยเทคนิคทางการทดลอง แต่การทดลองส่วนใหญ่มักถูกจำกัดโดยระดับความเข้มข้นสูง ซึ่งไม่สอดคล้องกับสภาวะการเกิดปฏิกิริยาจริงๆในระดับสารละลายความเข้มข้นต่ำ เพื่อแก้ปัญหาดังกล่าว การคำนวณโดยอาศัยแบบจำลองพลวัตเชิงโมเลกุลจึงถูกใช้เพื่อศึกษาสมบัติทางโครงสร้าง พลศาสตร์ และใช้อธิบายพฤติกรรมของระบบสารละลายในระดับโมเลกุลได้เป็นอย่างดี แบบจำลองพลวัตเชิงโมเลกุลส่วนใหญ่มักใช้เพียงการประมาณค่าแรงกระทำระหว่างอนุภาคแบบอันตรกิริยาคู่เท่านั้น การประมาณค่าด้วยฟังก์ชันศักย์ดังกล่าว อยู่บนพื้นฐานที่ว่าค่าอันตรกิริยาของอนุภาคที่มากกว่าสองอนุภาคมีค่าน้อยและไม่มีนัยสำคัญต่อแรงกระทำระหว่างอนุภาค ซึ่งผลจากการประมาณค่าดังกล่าวทำให้ค่าแรงดึงดูดระหว่างอนุภาคในระบบมีค่ามากเกินจริง โดยเฉพาะอย่างยิ่งระบบที่ประกอบด้วยไอออนโลหะประจุสูงรวมถึงสารประกอบไอออน จากผลงานวิจัยที่ผ่านมาพบว่า การใช้ฟังก์ชันศักย์ชนิดที่รวมอันตรกิริยาสามสามารถลดความผิดพลาดที่เกิดจากฟังก์ชันศักย์แบบอันตรกิริยาคู่ได้ โดยผลการคำนวณ เช่น การกระจายตัวในแนวรัศมี และ เลขโคออร์ดิเนชันของชั้นซอลเวชันที่ 1 มีค่าที่สอดคล้องกับผมการทดลอง แต่ยังไม่เพียงพอเนื่องจากไม่สามารถให้ค่าการกระจายตัวในแนวรัศมีและ เลขโคออร์ดิเนชันของชั้นซอลเวชันที่ 2 ที่สอดคล้องกับผลการทดลองได้ นอกจากนี้ ระบบสารละลายไอออนมีความซับซ้อนของแรงกระทำระหว่างหลายอนุภาคส่งผลให้การคำนวณแรงกระทำระหว่างอนุภาคสำหรับการสร้างฟังก์ชันศักย์ชนิดที่รวมอันตรกิริยาสามให้ครอบคลุมทุกการจัดเรียงตัวในสามมิติรวมถึงการประมาณค่าฟังก์ชันศักย์ดังกล่าวให้ได้คุณภาพที่ดีนั้นยังคงเป็นปัญหาสำคัญ เพื่อแก้ปัญหาดังกล่าว แบบจำลองพลวัตเชิงโมเลกุลแบบที่รวมวิธีทางกลศาสตร์ควอนตัมและทางกลศาสตร์โมเลกุลเข้าด้วยกันได้ถูกพัฒนาและนำมาใช้สำหรับศึกษาสมบัติทางโครงสร้างและพลศาสตร์ของไอออนในระบบสารละลาย โดยอาศัยแนวคิดที่ว่า ระบบในการศึกษาสามารถแบ่งออกได้เป็นส่วนๆ โดยแรงกระทำระหว่างอนุภาคในแต่ละส่วนสามารถอธิบายโดยการคำนวณทางกลศาสตร์ควอนตัมหรือกลศาสตร์โมเลกุลที่ระดับความถูกต้องแบบต่างๆ ยกตัวอย่าง เช่น ระบบที่ให้ความสำคัญกับชั้นซอลเวชันที่ 1 มากที่สุด อนุภาคที่อยู่ในบริเวณดังกล่าวจะถูกคำนวณด้วยระเบียบวิธีทางกลศาสตร์ควอนตัมซึ่งให้ผลการคำนวณที่มีความแม่นยำสูง ในขณะที่อนุภาคในส่วนที่เหลือของระบบจะถูกคำนวณด้วยระเบียบวิธีกลศาสตร์โมเลกุลซึ่งในที่นี้คือฟังก์ชันศักย์ชนิดต่างๆ เพื่อใช้สำหรับอธิบายแรงกระทำระหว่างอนุภาคในส่วนดังกล่าว ผลการคำนวณโดยระเบียบวิธีดังกล่าวจะให้ผลการคำนวณที่มีความแม่นยำสูง เนื่องจากทำการรวมแรงกระทำแบบหลายอนุภาค (many-body effect) ไว้แล้ว แต่อย่างไรก็ตามสำหรับระบบสารประกอบไอออนนั้น แบบจำลองพลวัตเชิงโมเลกุลแบบที่รวมวิธีทางกลศาสตร์ควอนตัมและทางกลศาสตร์

โมเลกุลเข้าด้วยกันยังคงมีปัญหา เนื่องจากยังคงต้องอาศัยฟังก์ชันศักย์เพื่ออธิบายแรงกระทำระหว่างอนุภาคที่อยู่นอกบริเวณที่คำนวณด้วยระเบียบวิธีทางกลศาสตร์ควอนตัม นอกจากนี้ การสร้างฟังก์ชันศักย์สำหรับระบบสารประกอบไอออนยังคงมีความซับซ้อนและยุ่งยาก เพื่อแก้ปัญหาดังกล่าว แบบจำลองพลวัตเชิงโมเลกุลที่รวมกลศาสตร์ควอนตัมในสนามประจุจึงถูกพัฒนาขึ้นเพื่อใช้สำหรับศึกษาระบบสารประกอบไอออนในระบบสารละลาย แบบจำลองพลวัตเชิงโมเลกุลที่รวมกลศาสตร์ควอนตัมในสนามประจุมีหลักการพื้นฐานมาจากแบบจำลองพลวัตเชิงโมเลกุลแบบที่รวมวิธีทางกลศาสตร์ควอนตัมและทางกลศาสตร์โมเลกุล แต่แบบจำลองพลวัตเชิงโมเลกุลที่รวมกลศาสตร์ควอนตัมในสนามประจุ ไม่จำเป็นต้องใช้ฟังก์ชันศักย์เพื่อใช้อธิบายแรงกระทำระหว่างอนุภาคในบริเวณกลศาสตร์ควอนตัมและบริเวณกลศาสตร์โมเลกุลอีกต่อไป เนื่องจากเทคนิคดังกล่าวจะคำนวณแรงกระทำของอนุภาคในบริเวณควอนตัมในสนามประจุของอนุภาคนอกบริเวณควอนตัม โดยผลการคำนวณที่ได้มีความสอดคล้องกับผลการทดลองเป็นอย่างดี

2. วิธีการทดลอง

1. หาเบซิสเซตที่เหมาะสำหรับการสร้างฟังก์ชันศักย์ (potential functions) ชนิด two- และ three-body potential functions สำหรับ V^{3+} และ H_2O

2. สร้างฟังก์ชันศักย์ชนิด two-body potential functions สำหรับ V^{3+}-H_2O และ three-body potential function สำหรับ H_2O-V^{3+}-H_2O

3. ทำการคำนวณแบบจำลองพลวัตเชิงโมเลกุลที่ใช้ฟังก์ชันศักย์แบบรวมอันตรกิริยาคู่ (two-body potential functions) ของสารละลายไอออนชนิด V^{3+} ในน้ำ

4. ทำการคำนวณแบบจำลองพลวัตเชิงโมเลกุลที่ใช้ฟังก์ชันศักย์แบบรวมอันตรกิริยาสาม (three-body potential function) ของสารละลายไอออนชนิด V^{3+} ในน้ำ

5. ทำการคำนวณแบบจำลองพลวัตเชิงโมเลกุลแบบที่รวมกลศาสตร์ควอนตัมและกลศาสตร์โมเลกุล (QM/MM) ของสารละลายไอออนชนิด V^{3+} ในน้ำ

6. ทำการคำนวณแบบจำลองพลวัตเชิงโมเลกุลที่รวมกลศาสตร์ควอนตัมในสนามประจุ (QMCF) ของระบบ HS^- HCl และ HSO_4^- ในน้ำ

6. วิเคราะห์หาสมบัติทางโครงสร้างและพลศาสตร์ของ V^{3+} HS^- HCl และ HSO_4^- ในน้ำ ที่ได้จากการคำนวณแบบจำลองพลวัตโมเลกุลแบบต่างๆ

3. ผลการทดลอง

3.1 วานาเดียมไอออน (V^{3+})

แบบจำลองพลวัตเชิงโมเลกุลแบบอันตรกิริยาคู่ของสารละลายไอออน V^{3+} ในน้ำมีเลขโคออร์ดิเนชันสำหรับชั้นซอลเวชันที่ 1 และ 2 เท่ากับ 8 และ 20 ตามลำดับ ซึ่งค่าที่ได้ดังกล่าวมีค่ามากกว่าค่าที่ได้จากผลการทดลอง (มีค่าเท่ากับ 6) ในขณะที่แบบจำลองพลวัตเชิงโมเลกุลแบบอันตรกิริยาสามให้ค่าดังกล่าวมีค่าเท่ากับ 6 และ 12.8 สำหรับชั้นซอลเวชันที่ 1 และ 2 ตามลำดับ โดยมีการกระจายตัวในแนวรัศมีของชั้นซอลเวชันที่ 1 และ 2 มีค่าเท่ากับ 1.99 และ 4.52 Å ตามลำดับ จากผลการคำนวณแสดงให้เห็นว่า การรวมแรงกระทำคู่สามมีความจำเป็นพื้นฐานสำหรับอธิบายสมบัติทางโครงสร้างในระบบสารละลายที่มีขนาดใหญ่และประจุสูง อย่างไงก็ตามแบบจำลองพลวัตเชิงโมเลกุลแบบอันตรกิริยาสามไม่สามารถใช้อธิบายความซับซ้อนของสมบัติทางโครงการได้ เช่น ในกรณีที่เกิดปรากฏการณ์ Jahn-Teller effects

สำหรับแบบจำลองพลวัตโมเลกุลที่รวมกลศาสตร์ควอนตัมและกลศาสตร์โมเลกุล (QM/MM) กระจายตัวในแนวรัศมี (V^{3+}-O) ของชั้นซอลเวชันที่ 1 และ 2 มีค่าเท่ากับ 1.99 และ 4.56 Å ตามลำดับ นอกจากนี้ยังตรวจพบปรากฏการณ์ Jahn-Teller effects โดยระยะทาง V^{3+}-O สำหรับแกน “equatorial” มีค่ารเท่ากับ 1.96 Å และ ระยะทาง V^{3+}-O สำหรับ “axial” มีค่าระยะทาง เท่ากับ 2.03 Å ซึ่งมีค่าใกล้เคียงกับค่าที่ได้จากการทดลองในระบบของแข็ง

3.2 ไบซัลไฟด์ (HS^-)

จากงานวิจัยพบกว่าค่าความยาวพันธะเฉลี่ยของ H-S มีค่าเท่ากับ 1.35 Å และมีการกระจายตัวในแนวรัศมีของชั้นซอลเวชันมีค่าเท่ากับ 2.42 Å สำหรับ $S_{HS^-}\cdots H_w$ และมีค่าเท่ากับ 3.97 Å สำหรับ $H_{HS^-}\cdots O_w$ โดยมีเลขโคออร์ดิเนชันสำหรับชั้นซอลเวชันมีค่าเท่ากับ 5.9 สำหรับด้านซัลเฟอร์อะตอม และมีค่าเท่ากับ 9.2 สำหรับด้านไฮโดรเจนอะตอม ค่าความถี่การสั่นสำหรับ $H_{HS^-}-S_{HS}$ มีค่าเท่ากับ 2752 cm^{-1} ซึ่งสอดคล้องกับค่าที่ได้จากการทดลอง (2570 cm^{-1}) จากผลการคำนวณแสดงให้เห็นว่าสารประกอบไบซัลไฟด์มีคุณสมบัติเป็น structure-making แบบอ่อน สอดคล้องกับค่าเวลาเฉลี่ยของการอยู่ในชั้นซอลเวชันเท่ากับ 1.5 และ 2.1 ps สำหรับด้านอะตอมซัลเฟอร์และไฮโดรเจน ตามลำดับ

3.3 กรดไฮโดรคลอริก (HCl)

ค่าความยาวพันธะเฉลี่ยของ H-Cl มีค่าเท่ากับ 1.28 Å คำนวณโดยแบบจำลองพลวัตเชิงโมเลกุลที่รวมกลศาสตร์ควอนตัมในสนามประจุ (QMCF) ซึ่งสอดคล้องกับค่าที่ได้จากการทดลองเป็นอย่างดี ค่าการกระจายตัวรัศมีของชั้นซอลเวชันสำหรับ $H_{HCl}\cdots O_w$ และ $Cl_{HCl}\cdots H_w$ มีค่าเท่ากับ 1.84 และ 3.51 Å ตามลำดับ เลขโคออร์ดิเนชันสำหรับชั้นซอลเวชันด้านไฮโดรเจนอะตอมมีค่าเท่ากับ 1 และมีค่าเท่ากับ 12 สำหรับด้านคลอไรด์อะตอม มีการตรวจพบการถ่ายโอนโปรตอน

ระหว่าง HCl และน้ำจำนวนสองครั้งตลอดเวลาการคำนวณแบบจำลองพลวัตเชิงโมเลกุลที่รวมกลศาสตร์ควอนตัมในสนามประจุ และ HCl มีคุณสมบัติ structure-making/breaking แบบอ่อน สอดคล้องกับค่าเวลาเฉลี่ยของการอยู่ในชั้นซอลเวชันเท่ากับ 2.1 และ 0.8 ps สำหรับด้านอะตอมคลอไรด์และไฮโดรเจน ตามลำดับ

3.4 ไบซัลเฟต (HSO_4^-)

แบบจำลองพลวัตเชิงโมเลกุลที่รวมกลศาสตร์ควอนตัมในสนามประจุ (QMCF) แสดงสมมาตรแบบ C_{3v} และมีค่าการสั่นที่สอดคล้องกับผลการทดลอง เลขโคออร์ดิเนชันสำหรับชั้นซอลเวชันมีค่าเท่ากับ 8.0 และ 10.9 แสดงการซ้อนทับปริมาตรของการหาค่าโคออร์ดิเนชันสำหรับสารประกอบไบซัลเฟต ค่าเฉลี่ยของการเกิดพันธะไฮโดรเจนตลอดเวลาการทำการคำนวณ 5.8 ps แสดงให้เห็นว่ามีโมเลกุลน้ำที่อยู่ในชั้นซอลเวชันเกิดพันธะไฮโดรเจนที่ไม่เสถียรกับสารประกอบไบซัลเฟต จากงานวิจัยยังพบว่า สารประกอบไบซัลเฟตมีคุณสมบัติ structure-making แบบอ่อน

4. บทวิจารณ์

งานวิจัยนี้แสดงให้เห็นว่า แบบจำลองพลวัตโมเลกุลแบบอันตรกิริยาคู่ไม่สามารถใช้อธิบายสมบัติทางโครงสร้างของสารละลายไอออนที่มีประจุสูงในน้ำได้ การรวมอันตรกิริยาคู่สามสามารถแก้ไขความผิดพลาดในการคำนวณแบบจำลองพลวัตโมเลกุลแบบอันตรกิริยาคู่ได้โดยแสดงค่าเลขโคออร์ดิเนชันที่สอดคล้องกับผลการทดลอง แต่ยังไม่เพียงพอยังสำหรับการอธิบาย ปรากฏการณ์ Jahn-Teller effects ที่เป็นลักษณะเด่นของสารละลายไอออนชนิด V^{3+} ได้ การคำนวณแบบจำลองพลวัตโมเลกุลที่รวมกลศาสตร์ควอนตัมและกลศาสตร์โมเลกุล (QM/MM) สามารถอธิบายสมบัติทางโครงสร้างรวมถึงปรากฏการณ์ Jahn-Teller effects ได้เป็นอย่างดีและสอดคล้องกับผลที่ได้จากการทำการทดลอง

แบบจำลองพลวัตเชิงโมเลกุลที่รวมกลศาสตร์ควอนตัมในสนามประจุ (QMCF) เป็นเทคนิคที่เหมาะสมสำหรับศึกษา HS^- HCl และ HSO_4^- ในน้ำ สมบัติทางโครงสร้างและพลศาสตร์มีค่าสอดคล้องกับค่าที่ได้จากการทดลองเป็นอย่างดี สารประกอบไบซัลไฟด์มีคุณสมบัติเป็น structure-making แบบอ่อน กรดไฮโดรคลอริกมีคุณสมบัติ structure-making/breaking แบบอ่อน ในขณะที่สารประกอบไบซัลเฟตมีคุณสมบัติ structure-making แบบอ่อน

5. เอกสารอ้างอิง

1. **Chinapong Kritayakornupong,** "Structural and Dynamical Properties of the V^{3+} Ion in Dilute Aqueous Solution: An Ab initio QM/MM molecular dynamics simulation" *J. Comput. Chem.*, **2009**; *30*: 2777-2783.

2. **Chinapong Kritayakornupong**; Viwat Vchirawongkwin; Bernd M. Rode, "Determination of Structure and Dynamics of the Solvated Bisulfide (HS^-) Ion by ab initio QMCF Molecular Dynamics",. *J. Phys. Chem. B* **2010**, *114*, 12883-12887.

3. **Chinapong Kritayakornupong**; Viwat Vchirawongkwin; Bernd M. Rode "Ab Initio quantum mechanical charge field molecular dynamics simulation of a dilute aqueous HCl solution", *J. Comput. Chem.* **2010**, *31*, 1785-1792.

4. Viwat Vchirawongkwin; **Chinapong Kritayakornupong**; Bernd M. Rode "Structural and Dynamical Properties and Vibrational Spectra of Bisulfate Ion in Water: A Study by Ab Initio Quantum Mechanical Charge Field Molecular Dynamics", *J. Phys. Chem. B* **2010**, *114*, 11564-11569.

6. Output จากโครงการวิจัยที่ได้รับทุนจาก สกว.

6.1 ผลงานตีพิมพ์ในวารสารวิชาการนานาชาติ

1. **Chinapong Kritayakornupong,** "Structural and Dynamical Properties of the V^{3+} Ion in Dilute Aqueous Solution: An Ab initio QM/MM molecular dynamics simulation" *J. Comput. Chem.*, **2009**; *30*: 2777-2783.

2. **Chinapong Kritayakornupong**; Viwat Vchirawongkwin; Bernd M. Rode, "Determination of Structure and Dynamics of the Solvated Bisulfide (HS^-) Ion by ab initio QMCF Molecular Dynamics",. *J. Phys. Chem. B* **2010**, *114*, 12883-12887.

3. **Chinapong Kritayakornupong**; Viwat Vchirawongkwin; Bernd M. Rode "Ab Initio quantum mechanical charge field molecular dynamics simulation of a dilute aqueous HCl solution", *J. Comput. Chem.* **2010**, *31*, 1785-1792.

4. Viwat Vchirawongkwin; **Chinapong Kritayakornupong**; Bernd M. Rode "Structural and Dynamical Properties and Vibrational Spectra of Bisulfate Ion in Water: A Study by Ab Initio Quantum Mechanical Charge Field Molecular Dynamics", *J. Phys. Chem. B* **2010**, *114*, 11564-11569.

6.2 การนำผลงานวิจัยไปใช้ประโยชน์

- เชิงสาธารณะ

มีเครือข่ายความร่วมมือระหว่างอาจารย์ ภาควิชาเคมี คณะวิทยศาสตร์ มหาวิทยาลัยเทคโนโลยีพระจอมเกล้าธนบุรี และ อาจารย์ ภาควิชาเคมี คณะวิทยศาสตร์ จุฬาลงกรณ์มหาวิทยาลัย

ภาคผนวก

Structural and Dynamical Properties of the V^{3+} Ion in Dilute Aqueous Solution: An *ab initio* QM/MM Molecular Dynamics Simulation

CHINAPONG KRITAYAKORNUPONG
Department of Chemistry, Faculty of Science, King Mongkut's University of Technology Thonburi, Bangkok, 10140 Thailand

Received 2 January 2009; Revised 18 February 2009; Accepted 26 February 2009
DOI 10.1002/jcc.21278
Published online 30 April 2009 in Wiley InterScience (www.interscience.wiley.com).

Abstract: A hybrid *ab initio* QM/MM molecular dynamics simulation at the Hartree-Fock level has been performed to investigate structural and dynamical parameters of the V^{3+} ion in dilute aqueous solution. A distorted octahedral structure with the average V^{3+}-O distance of 1.99 Å is evaluated from the QM/MM simulation, which is in good agreement with the X-ray data. Several structural parameters such as angular distribution functions, θ- and tilt-angle distributions have been determined to obtain the full description of the hydration structure of the hydrated V^{3+}. The Jahn-Teller distortions of the V^{3+} ion are pronounced in the QM/MM simulation. The mean residence time of 14.5 ps is estimated for the ligand exchange processes in the second hydration shell.

 J Comput Chem 30: 2777–2783, 2009

Key words: vanadium; Jahn-Teller effects; hydration structure; water exchange process; aqueous solution; QM/MM simulation; molecular dynamics simulation

Introduction

The aqua vanadium plays an essential role in chemical reactions and biological systems[1,2] since its complex has been used in the treatment of diabetes and cancer.[3,4] Because of the complexity of the V^{3+} ion in aqueous solution, it has been an interesting area for both experimental and theoretical studies.[5–18] In solution the hexahydrated V^{3+} is easily oxidized.[19] The oxygen-17 and proton magnetic resonance absorption were employed to investigate the coordination number and the water exchange processes in the hydration shell of vanadium(III) ion in aqueous solution. The six coordination number was observed with the water exchange between the first hydration shell and the bulk ($(\tau_M)_{25^\circ C} = 6.0 \times 10^{-4}$).[5] Crystal structures of the caesium alums[6] and the alkali–metal vanadium sulfate β-alums[7] were evaluated using the X-ray diffraction technique, providing the V^{3+}-O distances of 1.992 and 1.991 Å, respectively. The all-horizontal D_{3d} structure of the $[V(H_2O)_6]^{3+}$ complex in the $[V(H_2O)_6][H_5O_2](CF_3SO_3)_4$ structure was characterized using X-ray and neutron diffraction techniques, showing the V^{3+}-O bond distances reported in the range of 1.988–2.003 and 1.978–2.013 Å, respectively.[8] These observations are in contrast to T_h symmetry with the average V^{3+}-O bond distance of 2.063 Å predicted by *ab initio* SCF calculation.[9] Using the B3LYP/6-31+G*(5d,7f) level of theory,[10] the C_i symmetrical arrangement represents potential energy minima for V^{3+} aqua ion. Several spectroscopic techniques[11–16,20] were applied to evaluate the hydration structure and spectroscopic data of the V^{3+} ion in β-alums and salts. The distorted octahedral of the $[V(H_2O)_6]^{3+}$ ion was analyzed by low-temperature electronic spectra of $NH_4V(H_2O)_6(SO_4)\cdot 6H_2O$.[11] An electronic Raman method reveals the trigonal field splitting of the $^3T_{1g}$ ground term of hexa-vanadium(III) ion in the range of β-alums.[12] High-field multifrequency electron paramagnetic resonance (HF-EPR) spectroscopy has confirmed that the structure of the $[V(H_2O)_6]^{3+}$ complex is close to T_h symmetry.[16] Recently, numerous crystal structures of the $[V(H_2O)_6]^{3+}$ complex in different salts were investigated by X-ray and neutron diffraction methods,[17] showing that a variation of the V^{3+}-O bond distances is in the range from 1.987 to 2.004 Å. Subsequently, dynamical Jahn-Teller coupling in axially distorted vanadium(III) complex was also experimentally measured.[18]

The hydration structure and dynamical data of ions in dilute aqueous solutions have been successfully evaluated by molecular dynamics (MD) simulation techniques.[21–24] To describe the interactions between ion and water in the system, the approximation of pairwise additivity is generally applied. With the neglect of nonadditive terms (3, 4, ... , *N*-body) in pairwise

Correspondence to: C. Kritayakornupong; e-mail: chinapong.kri@kmutt.ac.th

Contract/grant sponsors: The Thailand Research Fund and Commission on Higher Education

Table 1. Final Optimized Parameters of the Analytical Pair Potential Functions and Three-Body Correction Function.[a]

Pair	A (kcal mol^{-1})	B (kcal mol^{-1})	C (kcal mol^{-1})	D (kcal mol^{-1})
V^{3+}-O	−18424.3945464 Å^5	33421.3216790 Å^6	−120720.9792811 Å^{11}	116488.5501479 Å^{12}
V^{3+}-H	1397.2693937 Å^4	−3096.6101911 Å^5	1760.4081494 Å^6	
3-body	A_1 (kcal/mol Å^4)	A_2 (Å^{-1})	A_3 (Å^{-1})	
O-V^{3+}-O	0.1936787	−0.0706336	0.5315865	

[a]Charges on O and H, taken from the CF2 water–water interaction potential, are −0.6598 and 0.3299, respectively.

additive approximation, the overestimations of hydration number especially for transition metal ions have been reported in several cases.[22,25] For highly charged metal ions, the inclusion of the three-body corrections is a basic requirement to determine the reliable structural data.[22,26] However, the inclusion of many-body contributions is demanded to provide an accurate description of dynamical properties for the hydrated metal ions.[27–31] To include the complicated many-body effects within the hydration shell of ions, the hybrid quantum mechanical/molecular mechanical (QM/MM) methods have been introduced[32,33] and lately applied to investigate structural and dynamical properties of various ions in solutions.[24,27–31,34–36] This technique describes the region of the main interest such as the ion's first hydration shell, by quantum mechanics, while the rest of the system consisting of solvent molecules is treated by *ab initio* constructed two-plus-three body potentials.

The objective of the present work was to determine structural and dynamical properties of V^{3+} in dilute aqueous solution by performing the classical and the QM/MM molecular dynamics simulations at the Hartree-Fock level. Several structural properties were evaluated in terms of radial distribution functions, coordination numbers, angular distributions, θ-angle distributions, and tilt angle distributions. In addition the mean ligand residence times were estimated for ligand exchange processes between the second hydration shell and the bulk of V^{3+}.

Methods

In the QM/MM MD simulation, the interactions within the MM region and between QM and MM regions are described by 2- and 3-body potential functions. The 2-body potential for the V^{3+}-H_2O interaction was newly constructed from *ab initio* quantum mechanical calculations at the unrestricted Hartree-Fock (UHF) level. The SBKJC VDZ ECP basis set,[37] omitting functions with the exponent below 0.5, was applied for V^{3+} to suppress the gas phase charge-transfer effect at larger V^{3+}-H_2O distance, and Dunning's DZP basis set[38,39] was used for O and H atoms of water. The similar methodology has been successfully applied in the previous ionic solutions.[30,40] However, a methodical test was also performed for the $[V(H_2O)_6]^{3+}$ cluster using different levels of theory with the identical basis sets as in the potential construction to ensure that our selected method is reliable. The average V^{3+}-O distance of 1.98 Å evaluated by the HF method is in good agreement with the experimental data.[6–8] This value is slightly longer than that observed from the MP2 method by 0.01 Å, whereas a shorter distance of 1.91 Å was obtained from the B3LYP method. The HF method gives the average binding energy of −129 kcal/mol, which is slightly lower than that elucidated from the MP2 method by 1 kcal/mol. On the other hand, the corresponding value of −134 kcal/mol was calculated from the B3LYP method. These results prove that the Hartree-Fock method is a suitable level of theory for studying the hydrated V^{3+} as a compromise between computational effort and accuracy of the results. More than 3300 unrestricted Hartree-Fock interaction energy points covering distances up to 12 Å and all angular orientations of the water were calculated by the TURBOMOLE 5.9 program[41–43] and fitted to an analytical form by a least square error minimization using the Levenberg-Marquardt algorithm to the following analytical formula:

$$\Delta E_{2bd} = \frac{A_O}{r^5_{V^{3+}-O}} + \frac{B_O}{r^6_{V^{3+}-O}} + \frac{C_O}{r^{11}_{V^{3+}-O}} + \frac{D_O}{r^{12}_{V^{3+}-O}} + \frac{q_O q_{V^{3+}}}{r_{V^{3+}-O}} + \sum_{i=1}^{2}\left(\frac{A_H}{r^4_{V^{3+}-H_i}} + \frac{B_H}{r^5_{V^{3+}-H_i}} + \frac{C_H}{r^6_{V^{3+}-H_i}} + \frac{q_H q_{V^{3+}}}{r_{V^{3+}-H_i}}\right), \quad (1)$$

where A, B, C, and D are fitting parameters, r is the distance between V^{3+} and the ith atom of H_2O, and q is the atomic net charges. The partial charges of −0.65966 and 0.32983 were applied for oxygen and hydrogen, respectively, according to the BJH-CF2 water model.[44,45] The experimental gas-phase[46] geometry of H_2O was fixed with the O—H distance of 0.9601 Å and the H—O—H angle of 104.47° during the energy calculations. The final optimized parameters are summarized in Table 1.

For a construction of 3-body potential function, 40,131 interaction points of the H_2O-V^{3+}-H_2O hypersurface were generated in the configuration space around V^{3+}. The resulting three-body corrections were fitted to the following functional form:

$$\Delta E_{3bd} = A_1 e^{-A_2(r_{V^{3+}-O_1} + r_{V^{3+}-O_2})} e^{(-A_3 r_{O_1-O_2})} \times (r_{CL} - r_{V^{3+}-O_1})^2 (r_{CL} - r_{V^{3+}-O_2})^2, \quad (2)$$

where A_1, A_2, and A_3 denote the fitting parameters, $r_{V^{3+}-O_1}$ and $r_{V^{3+}-O_2}$ are the vanadium-oxygen distances for water molecules one and two, respectively. $r_{O_1-O_2}$ represents the distance between the two oxygen atoms of the two water molecules. The cutoff limit r_{CL} of 6.0 Å is set, indicating that beyond such distance the three-body contributions become negligible. The fitting parameters of the three-body correction function for H_2O-V^{3+}-H_2O are also shown in Table 1.

Table 2. Characteristic Values of the Radial Distribution Functions, $g_{\alpha\beta}(r)$ for V^{3+} in Water.[a]

Solute	Ion/Water	r_{M1}	r_{m1}	n_1	r_{M2}	r_{m2}	n_2	Method	Reference
V^{3+}	1/499	1.98	2.28	8.0	4.03	5.10	~20	2-body MD	This work
V^{3+}	1/499	2.00	2.31	6.0	4.52	5.10	12.8	3-body MD	This work
V^{3+}	1/499	1.99/1.96/2.03	2.15	6.0	4.56	5.17	12.3	QM/MM MD	This work

[a] r_{M1}, r_{M2}, and r_{m1}, r_{m2} are the distances in Å, where $g_{\alpha\beta}(r)$ has the first and second maxima and the first and second minima, respectively. n_1 and n_2 are coordination numbers of the first and second hydration shells, respectively.

All classical molecular dynamic simulations have been performed in a canonical NVT-ensemble. A cubic periodic box with a side length of 24.7 Å containing one V^{3+} plus 499 water molecules was utilized. The temperature of the system was maintained at 298.16 K using the Berendsen algorithm.[47] The density of the simulation box was fixed at 0.997 g cm^{-3}, corresponding to the experimental value of pure water at 298.16 K. For the treatment of long-range electrostatic potentials and forces, the reaction field[48] was applied. Cutoff distances were set to 5 and 3 Å for non-Coulombic O—H and H—H interactions, respectively. For Coulombic interactions, a radial cutoff limit was set to half the box length. The intermolecular potential between H_2O molecules was described by the CF2 model[44] while the intramolecular potential of H_2O developed by Bopp et al. was used.[45] Since the BJH-CF2 water model[44,45] allows the explicit hydrogen movements, consequently the time step of 0.2 fs was chosen for the simulation.

In the QM/MM MD simulation, an *ab initio* quantum mechanical calculation was performed in each simulation step to provide the quantum mechanical forces inside the QM region. The total forces acting on each particle in the system was computed according to eq. (3)

$$F_{tot} = F_{MM}^{sys} + \left(F_{QM}^{QM} - F_{QM}^{MM}\right) * S_m(r) \tag{3}$$

where F_{MM}^{sys} is the forces of the whole system determined from the potential function, F_{QM}^{QM} is *ab initio* quantum mechanical forces inside the QM region, and F_{QM}^{MM} is the forces in the QM region evaluated from the potential function. r is the distance between the ion and the center of mass of the water molecule. For the water migrations between QM and MM regions, a smooth change of forces at the boundary has to be ensured by utilizing a smoothing function[49] S_m:

$$\begin{aligned} S_m(r) &= 1, && \text{for} \quad r \le r_1 \\ S_m(r) &= \frac{\left(r_0^2 - r^2\right)^2\left(r_0^2 + 2r^2 - 3r_1^2\right)}{\left(r_0^2 - r_1^2\right)^3}, && \text{for} \quad r_1 < r \le r_0 \\ S_m(r) &= 0, && \text{for} \quad r > r_0, \end{aligned} \tag{4}$$

where r_1 and r_0 are the distances characterizing the transition region, with a shell thickness of 0.2 Å.

A classical pair potentials molecular dynamics simulation was performed first, starting from a random configuration, followed by the inclusion of the 3-body corrections. The 3-body corrected simulation started from the equilibrium configuration of the pair potential simulation, then the system was re-equilibrated for 20 ps and a further 200 ps was used for the evaluations. Subsequently, the QM/MM molecular dynamics simulation was performed at the unrestricted Hartree-Fock (UHF) level using the identical basis sets as in the construction of the 2- and the 3-body correction functions. The value of 8.0 Å was chosen for the diameter of the QM region, including the first hydration shell and a small part of the second hydration shell of the V^{3+} ion determined from the three-body corrected simulation. The smoothing function[49] was thus applied between $r_1 = 3.8$ Å and $r_0 = 4.0$ Å. 4 ps was needed for re-equilibration, and a further 20 ps was processed to measure structural and dynamical properties.

Results and Discussion

Structural Properties

To describe the hydration structure of V^{3+} in aqueous solution, several structural parameters such as radial distribution functions (RDF), coordination numbers, and angular distributions were evaluated. Table 2 shows structural data elucidated from different types of molecular dynamics simulation. As expected, a classical simulation using pair potential functions gives an overestimated coordination number of 8. Figure 1 presents V^{3+}-O and V^{3+}-H RDFs and their corresponding integration numbers obtained from the QM/MM and 3-body corrected molecular dynamics simulations. Two distinct hydration shells are clearly observed from two well-defined peaks in the V^{3+}-O RDF obtained from both simulations. The first V^{3+}-O RDF peak reaches zero at ~4 Å, indicating that no water exchange processes occur between the first and second hydration shells. The QM/MM simulation shows a sharp first V^{3+}-O peak at 1.99 Å (with two weak shoulders at 1.96 and 2.03 Å), corresponding to an average coordination number of 6. The results of the QM/MM simulation are in good agreement with the experimental values in solid state.[6,7] The first shell distance of V^{3+} is slightly shorter than that evaluated for Ti^{3+} (with a mean distance of 2.08 Å obtained from 1-shell QM/MM simulation),[30] whereas it is slightly larger than the value of 1.92 Å determined for Cr^{3+}.[29] For 3-body corrected simulation, a less pronounced first V^{3+}-O peak is located at 1.99 Å, giving 6-coordinated complex for the first hydration shell. The lower intensity and broader shape of the first V^{3+}-O peak observed in the 3-body corrected simulation indicate a higher mobility of the ligand compared to the QM/MM simulation. For the second hydration shell, the maximum probability of the V^{3+}-O interaction was situated at 4.52 and 4.56 Å for the 3-body corrected and the QM/MM simulations, respectively. The V^{3+}-H RDF peak evaluated by the

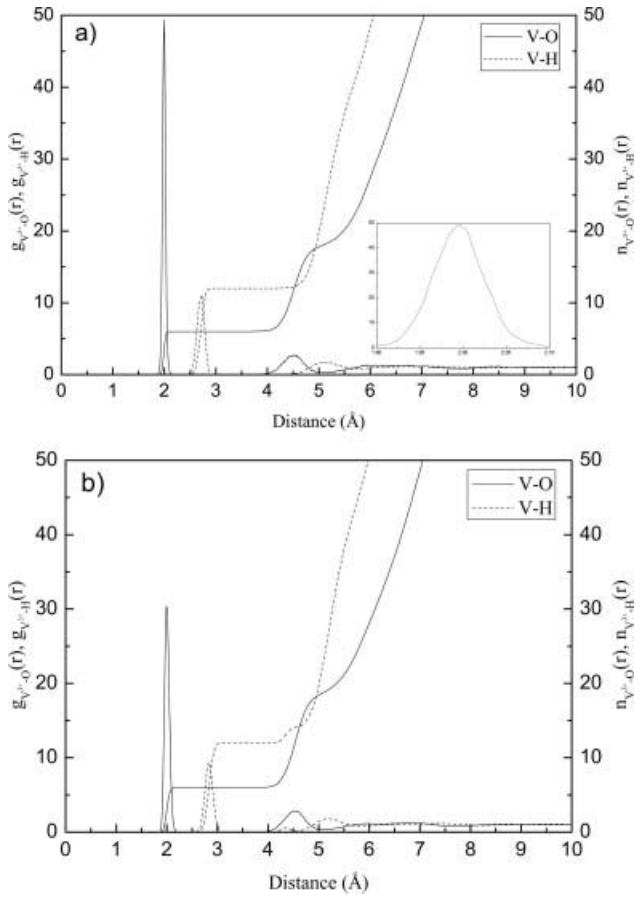

Figure 1. V^{3+}-O and V^{3+}-H radial distribution functions and their integrations obtained from (a) the QM/MM MD and (b) the three-body corrected MD simulations.

QM/MM simulation is centered at 2.72 Å for the first hydration shell, whereas the three-body corrected simulation reveals such peak at the larger distance of 2.83 Å. The splitting of the second-shell V^{3+}-H peak was exhibited in the 3-body corrected simulation, but it vanishes in the case of QM/MM simulation. The second-shell V^{3+}-H peaks are located at 5.10 and 5.21 Å determined from the QM/MM and three-body corrected simulations, respectively. These results indicate that a classical simulation with *ab initio* generated 2 + 3-body potentials is insufficient for evaluating hydration structure of this highly charged metal ion in aqueous solution. A QM/MM simulation gives an accurate description for structural properties.

Figure 2 shows the probability distribution of coordination numbers of the hydrated V^{3+} ion for the first and second hydration shells, obtained from the QM/MM and the 3-body corrected simulations. An exact coordination number of 6 for the first hydration shell were evaluated from both simulations. Different results in the coordination numbers between the QM/MM and the 3-body corrected simulations were pronounced in the second solvation shell. The three-body corrected simulation favors a coordination number of 13 (followed by 12 and 14 with 37 and 16% occurrence, respectively). The QM/MM simulation gives the coordination number ranging from 10 to 15 with 12 presenting the most dominant. This proves that one water molecule in the first hydration shell is bound to two second-shell ligands.

Figure 3 displays the O-V^{3+}-O angular distributions for the first hydration shell, calculated up to the first minimum of the V^{3+}-O RDFs. Two O-V^{3+}-O peaks with the maximum values at 90 and 176° were derived from the QM/MM simulation. The three-body corrected simulation gives the similar values of 89 and 175°. These reflect the structure of a distorted octahedron obtained from both simulations.

The geometrical arrangement of water molecule around the V^{3+} ion is quite an interesting information to observe the influenced quantum corrections in the hydration shell. Therefore, two different angles were defined: angle θ is the angle between the vector pointing along the V—O axis and the dipole vector of the water, and Tilt angle is the angle between the V—O axis and the plane defined by the O—H vectors. Figure 4 illustrates the angle θ and the tilt distributions of water molecules in the first hydration shell obtained from the QM/MM and the three-body

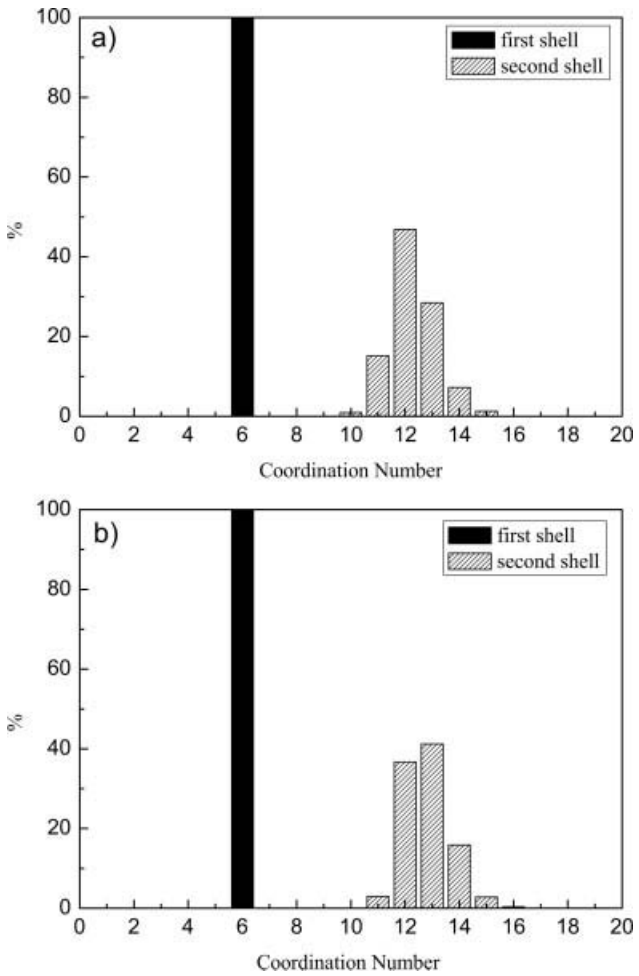

Figure 2. The first and second shell coordination number distributions of the hydrated V^{3+}, obtained from (a) the QM/MM MD and (b) the three-body corrected MD simulations.

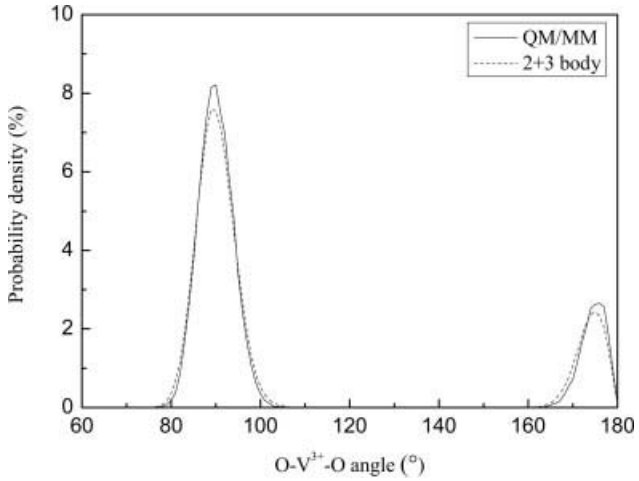

Figure 3. Distributions of the O-V^{3+}-O angles for the first hydration shell, obtained from the QM/MM MD and the three-body corrected MD simulations.

corrected simulations. The maximum value of 174° for the distribution of the angle θ was elucidated from both simulations. However, ligands with the quantum mechanical treatment are more rigid than those in the case of 3-body corrections. The less flexibility of the solvated ligands in the QM/MM simulation was also detected by a narrower peak showing with its maximum at +1° reaching zero at ±15°. In contrast a rather broad peak ranging from −25 to +25° with its maximum at −1° was estimated from the three-body corrected simulation.

Jahn-Teller Effects

The Jahn-Teller effects of hydrated V^{3+} are quite complex and have been investigated in the solid phase using spectroscopic techniques.[12,13,16,18,20] To our knowledge, no structural data has been evaluated for the Jahn-Teller distortions of the V^{3+} ion in aqueous solution. The QM/MM simulation has proved to be a suitable tool to study the dynamic aspects of Jahn-Teller distortions of hydrated ions in the picosecond time range.[30,36,50,51] The Jahn-Teller distortion of the $[V(H_2O)_6]^{3+}$ complex is shown in the first peak of V^{3+}-O RDF obtained from the QM/MM simulation (see Fig. 1). This first peak shows the weak shoulders at 1.96 and 2.03 Å, corresponding to the average V^{3+}-O distances of the "equatorial" and "axial" ligands, respectively. Figure 5 displays the fast V^{3+}-O bond-length changes in the first hydration shell during the simulation time of 20 ps. The QM/MM simulation reveals the fast dynamics and irregularity of Jahn-Teller distortions of the $[V(H_2O)_6]^{3+}$ complex, indicating three different pairs of the opposite ligands (a–b, c–d, and e–f, see Fig. 5). The variation of the V^{3+}-O distances is in the range of 1.9–2.1 Å, which is almost the same as that determined for Ti^{3+} (1.9–2.2 Å).[30] In addition, the QM/MM molecular dynamics simulations reveal the real time picture of the Jahn-Teller distortions. The long-time distortion of ~7 ps, which is the time for the average ion-ligand distance reaching both "equatorial" and axial values, was estimated in the case of V^{3+}. Such value is slightly shorter than that evaluated for Ti^{3+}(8.5 ps).[30] These indicate the longer of Jahn-Teller inversion times for the trivalent transition metal ions compared to those for the divalent transition metal ions. (1-4 ps for Cr^{2+}, 3-5.5 ps for Cu^{2+}, and 2-3 ps for Ag^{2+}).[36,50,51]

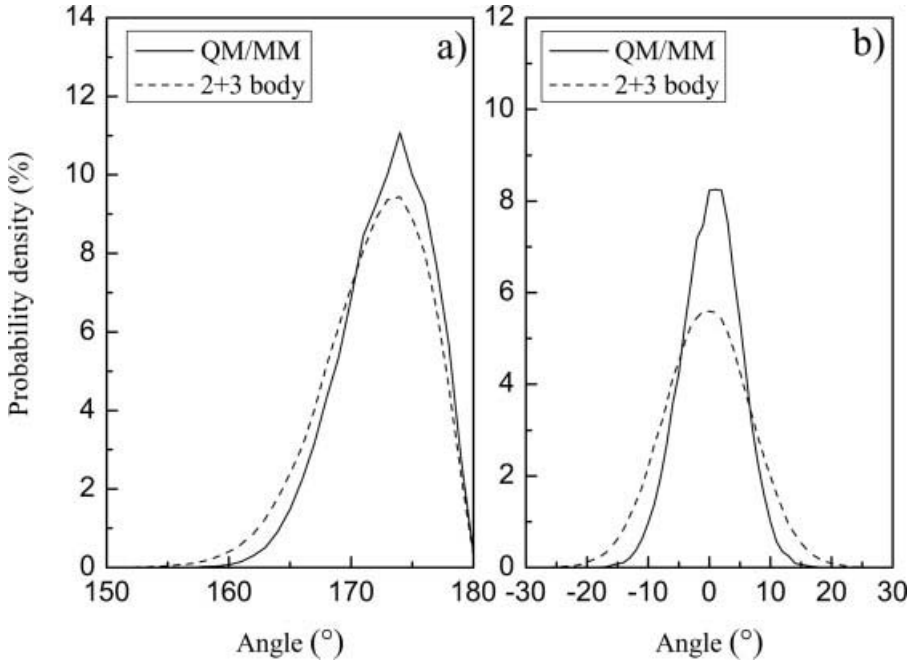

Figure 4. Angular V^{3+}-H_2O configuration for the first hydration shell, a) θ angle and b) Tilt angle distributions, obtained from the QM/MM MD and the three-body corrected MD simulations.

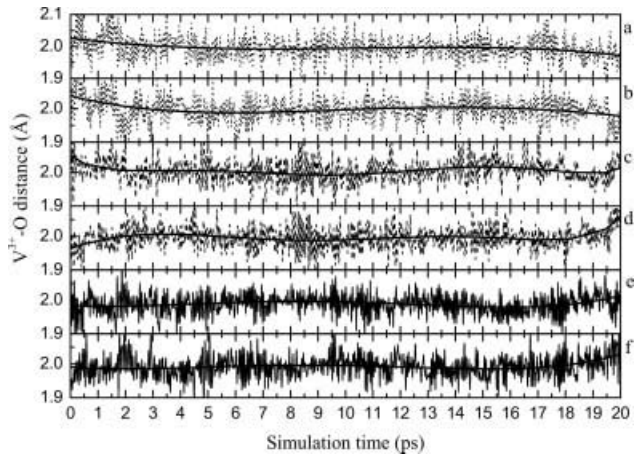

Figure 5. The distances of V^{3+}-O in the first hydration shell obtained from the QM/MM MD simulation.

Ligand Exchange Processes

In order to investigate the mobility of ligands in the hydration shells, the mean residence times (MRT) were calculated using the 'direct method.'[52] In this method, a direct accounting for a ligand remaining inside/outside the hydration shell for $t^* = 0$ and 0.5 ps is calculated. As expected, no water exchange processes between the first and second hydration shells were observed, while numerous water exchange processes were detected in the second hydration shell as shown in Figure 6. Therefore, only the MRT values for the second hydration shell were examined and summarized in Table 3. The QM/MM simulation gives the MRT values of 1.0 ps for $t^* = 0$ and 14.5 ps for $t^* = 0.5$ ps, corresponding to 243 and 17 exchange processes in the second hydration shell, respectively. The MRT value

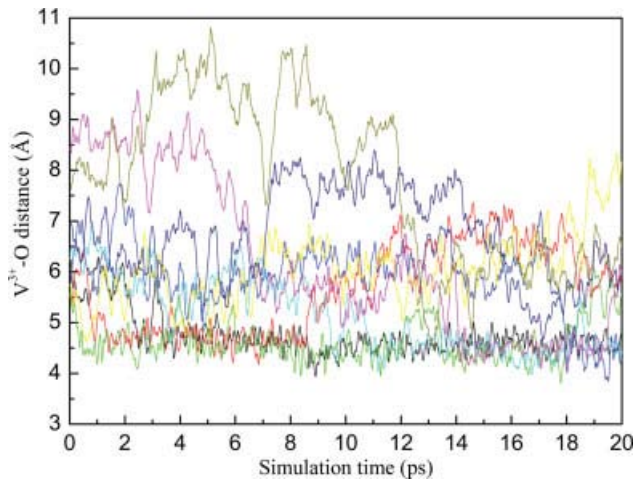

Figure 6. Distributions of the V^{3+}-O distances during the QM/MM simulation showing numerous exchange processes between the second hydration shell and the bulk.

Table 3. Mean Ligand Residence Times and Sustainability of Migration Processes to and from the Second Hydration Shell of V^{3+}.

		$t^* = 0$ ps		$t^* = 0.5$ ps			
Solute	t_{sim}	N_{ex}^0	$\tau_{H_2O}^0$	$N_{ex}^{0.5}$	$\tau_{H_2O}^{0.5}$	S_{ex}	$1/S_{ex}$
V^{3+}	20.0	243	1.0	17	14.5	0.07	14.3
Bulk[a]	10.0	269	0.2	24	1.7	0.09	11.2

[a]Values obtained from a QM/MM MD simulation of pure water.[51]

of 14.5 ps obtained from V^{3+} is much shorter than the value of 37 ps evaluated for Ti^{3+} (with 2-shell QM/MM simulation applied), showing more frequent ligand exchange processes. Since the MRT values estimated with $t^* = 2.0$ ps of Cr^{3+} and Fe^{3+} are 22.4 and 39.7 ps, respectively,[52] the corresponding value of 27.3 ps was also elucidated for V^{3+}. The results show that the ligand exchange processes in the case of V^{3+} are considerably slower than those of Cr^{3+}, but they are faster than those observed in the case of Fe^{3+}. In addition, the sustainability of the exchange processes (S_{ex}) is determined by comparing the number of all transitions through a shell boundary (N_{ex}^0) to the number of the exchange events lasting at least 0.5 ps ($N_{ex}^{0.5}$). The inverse of the sustainability coefficient indicates the average number of attempts leading to a successful exchange event in the hydration shell of the ion. The QM/MM simulation gives the values of 0.07 and 14.3 for S_{ex} and $1/S_{ex}$, respectively.

Conclusions

The hydration structure and dynamics data of the V^{3+} ion in dilute aqueous solution were investigated using a classical and the QM/MM molecular dynamics simulation. An exact coordination number of 6 for the first hydration shell were obtained from both simulation techniques. The 3-body corrected simulation exhibits a correct coordination number for the first hydration shell, but it fails to reproduce the Jahn-Teller effect of the hydrated V^{3+}. The QM/MM simulation is a powerful tool to obtain an accurate description of structural and dynamical data for the hydrated V^{3+}. The structural properties obtained from the QM/MM simulation are in good agreement with the experimental techniques. The less flexibility of the solvated ligands was observed in the case of QM/MM simulation compared to the 3-body corrected simulation. The Jahn-Teller distortions of the $[V(H_2O)_6]^{3+}$ complex were observed in the QM/MM simulation with the inversion time of ~7 ps, indicating a slightly shorter value than the corresponding one estimated for Ti^{3+}. Several ligand exchange reactions in the second hydration shell yielded the mean residence time of 14.5 ps. To obtain a more accurate description of dynamics of the Jahn-Teller effect of V^{3+}, the inclusion of the second hydration shell into the QM region is needed. However, such 2-shell *ab initio* QM/MM molecular dynamics simulation is extremely time-demanding for long simulation times, which at least 10 ps is required for the evaluation.

References

1. Crans, D. C.; Smee, J. J.; Gaidamauskas, E.; Yang, L. Chem Rev 2004, 104, 849.
2. Meier, R.; Boddin, M.; Mitzenheim, S.; Kanamori, K. Met Ions Biol Syst 1995, 31, 45.
3. Sakurai, H. Clin Calcium 2005, 15, 49.
4. Thompson, K. H.; Orvig, C. Met Ions Biol Syst 2004, 41, 221.
5. Chmelnick, A. M.; Fiat, D. J Mag Res 1972, 8, 325.
6. Beattie, J. K.; Best, S. P.; Skelton, B. W.; White, A. H. J Chem Soc Dalton Trans 1981, 2105.
7. Beattie, J. K.; Best, S. P.; Favero, P. D.; Skelton, B. W.; Sobolev, A. N.; White, A. H. J Chem Soc Dalton Trans 1996, 1481.
8. Cotton, F. A.; Fair, C. K.; Lewis, G. E.; Mott, G. N.; Ross, F. K.; Schultz, A. J.; Williams, J. M. J Am Chem Soc 1984, 106, 5319.
9. Åkesson, R.; Pettersson, L. G. M.; Sandström, M.; Wahlgren, U. J Am Chem Soc 1994, 116, 8691.
10. Kallies, B.; Meier, R. Inorg Chem 2001, 40, 3101.
11. Hitchman, M. A.; McDonald, R. G.; Smith, P. W.; Stranger, R. J Chem Soc Dalton Trans 1988, 1393.
12. Best, S. P.; Clark, R. J. H. Chem Phys Lett 1985, 122, 401.
13. Tregenna-Piggott, P. L. W.; Best, S. P.; Güdel, H.-U.; Weihe, H.; Wilson, C. C. J Solid State Chem 1999, 145, 460.
14. Tregenna-Piggott, P. L. W.; Weihe, H.; Bendix, J.; Barra, A.-L.; Güdel, H.-U. Inorg Chem 1999, 38, 5928.
15. Spichiger, D.; Carver, G.; Dobe, C.; Bendix, J.; Tregenna-Piggott, P. L. W.; Meier, R.; Zahn, G. Chem Phys Lett 2001, 337, 391.
16. Dolder, S.; Spichiger, D.; Tregenna-Piggott, P. L. W. Inorg Chem 2003, 42, 1343.
17. Tregenna-Piggott, P. L. W.; Spichiger, D.; Carver, G.; Frey, B. Inorg Chem 2004, 43, 8049.
18. Tregenna-Piggott, P. L. W.; Carver, G. Inorg Chem 2004, 43, 8061.
19. Vilas Boas, L. F.; Costa Pessoa, J. In Comprehensive Coordination Chemistry; Wilkinson, G., Gillard, R. D., McCleverty, J. A., Eds.; Pergamon: Oxford, 1987; Vol. 3, Chapter 33, p 453.
20. Tregenna-Piggott, P. L. W.; Best, S. P. Inorg Chem 1996, 35, 5730.
21. Helm, L.; Merbach, A. E. Coord Chem Rev 1999, 187, 151.
22. Kritayakornupong, C.; Yagüe, J. I.; Rode, B. M. J Phys Chem A 2002, 106, 10584.
23. Blumberger, J.; Bernasconi, L.; Tavernelli, I.; Vuilleumier, R.; Sprik, M. J Am Chem Soc 2004, 126, 3928.
24. Rode, B. M.; Schwenk, C. F.; Hofer, T. S.; Randolf, B. R. Coord Chem Rev 2005, 249, 2993.
25. Marini, G. W.; Texler, N. R.; Rode, B. M. J Phys Chem 1996, 100, 6808.
26. Durdagi, S.; Hofer, T. S.; Randolf, B. R.; Rode, B. M. Chem Phys Lett 2005, 406, 20.
27. Kritayakornupong, C.; Plankensteiner, K.; Rode, B. M. J Phys Chem A 2003, 107, 10330.
28. Kritayakornupong, C.; Plankensteiner, K.; Rode, B. M. J Chem Phys 2003, 119, 6068.
29. Kritayakornupong, C.; Plankensteiner, K.; Rode, B. M. J Comput Chem 2004, 25, 1576.
30. Kritayakornupong, C.; Plankensteiner, K.; Rode, B. M. ChemPhysChem 2004, 5, 1499.
31. Kritayakornupong, C.; Rode, B. M. J Chem Phys 2003, 118, 5065.
32. Warshel, A.; Levitt, M. J Mol Biol 1976, 103, 227.
33. Singh, U. C.; Kollman, P. A. J Comput Chem 1986, 7, 718.
34. Kritayakornupong, C. Chem Phys Lett 2007, 441, 226.
35. Kritayakornupong, C.; Hannongbua, S. Chem Phys 2007, 332, 95.
36. Kritayakornupong, C. J Comput Chem 2008, 29, 115.
37. Stevens, W. J.; Krauss, M.; Basch, H.; Jasien, P. G. Can J Phys 1992, 70, 612.
38. Dunning, T. H., Jr.; Wadt, W. R. J Chem Phys 1989, 90, 1007.
39. Dunning, T. H., Jr.; Hay, P. J. In Modern Theoretical Chemistry: Methods of Electronic Structure Theory; Schaefer, H. F., III, Ed.; Plenum Press: New York, 1977; Vol. 3.
40. Hofer, T. S.; Randolf, B. R.; Rode, B. M. Phys Chem Chem Phys 2005, 7, 1382.
41. Ahlrichs, R.; Bär, M.; Häser, M.; Horn, H.; Kölmel, C. Chem Phys Lett 1989, 162, 165.
42. Ahlrichs, R.; von Arnim, M. Methods and Techniques in Computational Chemistry: METECC-95; Cagliari, Sardinia, 1995.
43. von Arnim, M.; Ahlrichs, R. J Comput Chem 1998, 19, 1746.
44. Stillinger, F. H.; Rahman, A. J Chem Phys 1978, 68, 666.
45. Bopp, P.; Janscó, G.; Heinzinger, K. Chem Phys Lett 1983, 98, 129.
46. Kuchitsu, K.; Morino, T.; Maeda, M. Bull Chem Soc Jpn 1976, 49, 701.
47. Berendsen, H. J. C.; Postma, J. P. M.; van Gunsteren, W. F.; DiNola, A.; Haak, J. R. J Phys Chem 1984, 81, 3684.
48. Adams, D. J.; Adams, E. H.; Hills, G. J Mol Phys 1979, 38, 387.
49. Brooks, B. R.; Bruccoleri, R. E.; Olafson, B. D.; States, D. J.; Swaminathan, S.; Karplus, M. J Comput Chem 1983, 4, 187.
50. Kritayakornupong, C. J Comput Chem 2008, 445, 207.
51. Schwenk, C. F.; Rode, B. M. ChemPhysChem 2003, 4, 931.
52. Hofer, T. S.; Tran, H. T.; Schwenk, C. F.; Rode, B. M. J Comput Chem 2004, 25, 211.

Determination of Structure and Dynamics of the Solvated Bisulfide (HS^-) Ion by ab Initio QMCF Molecular Dynamics

Chinapong Kritayakornupong,*,† Viwat Vchirawongkwin,‡ and Bernd M. Rode§

Department of Chemistry, Faculty of Science, King Mongkut's University of Technology Thonburi, Bangkok, 10140 Thailand, Department of Chemistry, Faculty of Science, Chulalongkorn University, Bangkok, 10330 Thailand, and Theoretical Chemistry Division, Institute of General, Inorganic and Theoretical Chemistry, University of Innsbruck, Innrain 52a, A-6020 Innsbruck, Austria

Received: May 27, 2010; Revised Manuscript Received: August 13, 2010

The hydration structure of the bisulfide (HS^-) ion in dilute aqueous solution was characterized by means of an ab initio quantum mechanical charge field (QMCF) molecular dynamics simulation at the Hartree−Fock level employing Dunning double-ζ plus polarization function (DZP) basis sets. An average H−S bond distance of 1.35 Å resulted from the simulation and a hydration shell located at 2.42 Å $S_{HS^-}\cdots H_w$ and 3.97 Å HS^- distances, respectively. At the sulfur site, the average coordination number is 5.9 ± 1.1, while the value for the hydrogen site is 9.2 ± 1.6. The calculated $H_{HS^-}-S_{HS^-}$ stretching frequency of 2752 cm^{-1} obtained from the QMCF MD simulation is in good agreement with that reported from the Raman spectrum (2570 cm^{-1}) only if a scaling factor of 0.89 is applied. The stability of the nondissociated HS^- structure is reflected by the force constants of 436.1 and 4.5 N/m determined for the $H_{HS^-}-S_{HS^-}$ and $H_{HS^-}\cdots O_w$ bonds, respectively. A weak structure-making effect of the hydrated HS^- ion results from the mean residence times of 1.5 and 2.1 ps of coordinated water molecules at the sulfur and hydrogen sites of the HS^- ion, respectively.

1. Introduction

The chemistry of sulfide ions is an interesting area, not only in the fundamental chemistry and electrochemistry of numerous salts[1] but also in atmospheric pollution as a constituent of the sulfur cycle,[2] petroleum hydrodesulfurization processes, as well as paper and pulp industries. In aqueous solution, bisulfide (HS^-) ion can be obtained from the dissolved hydrogen sulfide (H_2S) with a suggested pK_1 value of 7.01,[3] while the subsequent dissociation of the bisulfide leads to the sulfide (S^{2-}) ion, characterized by large experimental values of pK_2 in the wide range 12.5−18.5.[4−11] For example, Stephens and Cobble[5] presented a value of 13.78, Licht et al.[8] reported a value of 17.1, and Migdisov et al.[9] selected a value of 17.4 at 25 °C. All of these indicate that HS^- exists as a major species in aqueous H_2S solution, while minor activities of S^{2-} only occur in extremely high ionic strength solutions.[8] In general, HS^- acts as a Lewis base, whereas H_2S can behave as a Lewis base or acid. Due to the dominance of bisulfide ion in aqueous solution, several experiments confirmed that the bisulfide ion acts as the initial species to form metal hydrosulfide in the precipitation of metal sulfide from solution, which is of great environmental interest.[12,13] To our knowledge, no structural analysis of the HS^- ion in aqueous solution has been performed by experimental techniques, only the H−S vibrational frequency of 2570 cm^{-1} was determined by Raman spectroscopy.[7] For theoretical investigations, there have been a few calculations aimed at the structure and stability of $[H_2S(H_2O)]_n$ clusters,[14−18] which are not directly relevant for the solvated HS^- ion.

Recently, the quantum mechanical charge field (QMCF) molecular dynamics simulation approach has been developed,[19] presenting a suitable tool to investigate composite and asymmetrical ions in aqueous solution,[20−23] since the first and second hydration layers are included in the quantum mechanical treatment. In our previous publications,[21,22] structural and dynamical properties of aqueous HF and HCl solutions were successfully studied using this technique. Therefore, it was of great interest to characterize the hydration structure as well as the dynamical behavior of the analogous HS^- compound with its extremely weak acid behavior in aqueous solution by employing the QMCF MD methodology.

In the present work, an ab initio quantum mechanical charge field molecular dynamics simulation at the Hartree−Fock level was performed for a system consisting of one HS^- ion plus 498 water molecules. To characterize the hydration structure of the hydrated HS^- ion, numerous structural parameters such as radial distribution functions, coordination numbers, angular distributions, θ angle, and tilt angle distributions were determined. The vibrational frequency of the H−S bond was determined to compare it with the experimental value, while the $H_{HS^-}\cdots O_w$ vibrational mode was calculate to describe the hydrogen bond strength between solute and water molecules. Subsequently, dynamics of ligand exchange processes between hydration shell of the HS^- ion and bulk were analyzed on the basis of the mean residence times.

2. QMCF MD Simulation

The quantum mechanical charge field (QMCF) molecular dynamics simulation[19,24] is a technique based on a partitioning scheme similar to conventional QM/MM MD methods,[25−27] which divides the system into two parts (QM and MM regions) where different levels of theory are appropriately applied. In the QMCF technique, the QM region using the ab initio quantum mechanical calculation is extended to include the second hydration shell and also splits into two subregions, which are

* Corresponding author. Fax: +66(2)470-8962. E-mail:chinapong.kri@kmutt.ac.th.
† King Mongkut's University of Technology Thonburi.
‡ Chulalongkorn University.
§ University of Innsbruck.

10.1021/jp104856q
Published on Web 09/21/2010

the core region containing the solute and the first solvation shell and the solvation layer containing only solvent molecules. In addition, the QMCF technique describes the Coloumbic interactions of the solute with bulk solvent molecules by quantum chemically evaluated partial charges of the atoms in the QM region and the point charges of the atoms in the MM region. The charges of the MM particles also enter as a perturbation term into the core Hamiltonian:

$$H_{CF} = H_{HF} + V_i' \tag{1}$$

$$V_i' = \sum_{j=1}^{M} \frac{q_j}{r_{ij}} \tag{2}$$

where q_j are the partial charges of each atom in the MM region as defined in the used water model BJH-CF2,[28,29] i.e., −0.65966 and +0.32983 for oxygen and hydrogen, respectively. Consequently, the forces acting on each particle in the different regions are defined as

$$F_j^{core} = F_j^{QM} + \sum_{i=1}^{M} \frac{q_j^{QM} q_i^{MM}}{r_{ij}^{\,2}} \tag{3}$$

$$F_j^{layer} = F_j^{QM} + \sum_{i=1}^{M} \frac{q_j^{QM} q_i^{MM}}{r_{ij}^{\,2}} + \sum_{i=1}^{M} F_{ij}^{BJHnC} \tag{4}$$

$$F_j^{MM} = \sum_{\substack{i=1 \\ i \neq j}}^{M} F_{ij}^{BJH} + \sum_{i=1}^{N_1+N_2} \frac{q_i^{QM} \cdot q_j^{MM}}{r_{ij}^{\,2}} + \sum_{i=1}^{N_2} F_{ij}^{BJHnC} \tag{5}$$

where F_j^{core}, F_j^{layer}, and F_j^{MM} are the forces acting on particle j situated in the core region, the solvation layer, and the MM region, respectively. M is the number of atoms in the MM region. In each simulation step, the ab initio quantum mechanical forces in core and layer regions (F_j^{core} and F_j^{layer}) are evaluated in conjunction with the Coulombic forces obtained from all particles in the MM region. The non-Coulombic forces between the core particles and the MM particles are neglected, justified by the distance between the core and the MM region of at least 3 Å, while the QM forces in the layer (F_j^{layer}) are supplemented by the non-Coulombic forces of particles in the MM region according to the BJH-CF2 water model.[28,29] Consequently, the forces in the MM region (F_j^{MM}) are determined by the BJH-CF2 water model[28,29] augmented by the Coulombic forces exerted by all particles in the core region (N_1) and the layer region (N_2), and the non-Coulombic forces (F_{ij}^{BJHnC}) generated by the particles in the layer region (N_2).

During the QMCF MD simulation, the migration of solvent molecules between the QM and MM region can occur frequently. To ensure a continuous transition of forces at the boundary, the forces acting on each particle in the system can be defined as

$$F_j^{Smooth} = F_j^{MM} + (F_j^{layer} - F_j^{MM}) \cdot S_m(r) \tag{6}$$

where $F_j^{MM}$and F_j^{layer} are the forces acting on the particle j in the MM region and located in the solvation layer, respectively, r is the distance of the water molecule from the sulfur atom of the HS^- ion, and S_m is a smoothing function,[30]

$$\begin{aligned} S_m(r) &= 1 && \text{for } r \le r_1 \\ S_m(r) &= \frac{(r_0^{\,2} - r^2)^2 (r_0^{\,2} + 2r^2 - 3r_1^{\,2})}{(r_0^{\,2} - r_1^{\,2})^3} && \text{for } r_1 < r \le r_0 \\ S_m(r) &= 0 && \text{for } r > r_0 \end{aligned} \tag{7}$$

where r_1 is the inner border of the smoothing region and r_0 is the radius of the QM region. Further details of the method are presented in refs 19 and 24.

The QMCF MD simulation of the bisulfide ion in aqueous solution was performed in a 24.7 Å × 24.7 Å × 24.7 Å periodic boundary cubic box, consisting of one HS^- ion plus 498 water molecules. The canonical *NVT* ensemble was controlled by the Berendsen temperature-scaling algorithm[31] using a relaxation time of 100 fs to keep the temperature at 298.15 K. The density of the simulation was fixed at 0.997 g cm^{-3}, corresponding to the experimental value of pure water at this temperature. The time step of the predictor-corrector algorithm was set to 0.2 fs, enabling an explicit description of hydrogen movements. The flexible BJH-CF2 water model[28,29] for the MM region also enables explicit hydrogen movements, thus ensuring a smooth transition of water molecules between QM and MM region. Cutoff distances of 5 and 3 Å were used for non-Coulombic O−H and H−H interactions, respectively. The radial cutoff limit for Coulombic interactions was set to half the box length and the reaction field[32] was applied to correct for long-range Coulombic interactions. The radius of the core region was chosen as 3.0 Å with the layer region ranging from 3.0 to 5.7 Å in which the smoothing function[30] was applied between r_0 (5.7 Å) and r_1 (5.5 Å). The TURBOMOLE 5.9 program[33−35] was employed to evaluate the forces in the QM region calculated at the restricted Hartree−Fock (RHF) level. Dunning double-ζ plus polarization function (DZP) basis sets[36−38] were applied for sulfur, oxygen, and hydrogen atoms. A methodical test was performed for a comparison of the geometric parameters obtain from the HF method optimization of $[HS(H_2O)_n]^-$ ($n = 0-6$) clusters with and without diffuse functions of the DZP basis set. It was found that the average H−S distances determined by the HF/DZP+ method are slightly shorter by ∼0.002 Å than those evaluated from the HF/DZP method. In addition, the H−S distance in the $[HS(H_2O)_4]^-$ cluster is 1.3333 Å calculated from the HF/DZP method, which is in good agreement with that evaluated from the MP2/6-31+G(d,p) method (1.33 Å).[16] These prove that the diffuse functions can be neglected. The initial configuration was taken from the simulation of the HF molecule. After equilibration of 6 ps, a 10 ps run was used for sampling. To ensure that true equilibrium had been established, the sampling trajectory was separately evaluated for the first and second 5 ps. The simulation protocol applied in this work is similar to that utilized in previous simulations of aqueous HF and HCl solutions.[21,22]

Similar to the HF and HCl molecules, the HS^- ion has the $C_{\infty v}$ symmetry, indicating that vibrational motion of the HS^- ion is both infrared- and Raman-active. Velocity autocorrelation functions (VACFs) were evaluated to gain access to the vibrational spectrum of the HS^- ion in aqueous solution. The velocity of the hydrogen atom was projected onto a unit vector parallel to the corresponding S−H bond ($\vec{\mathbf{u}}_1$), while the vibrational mode ν is the projection of the hydrogen velocity onto the unit vector $\vec{\mathbf{u}}_1$. The vibrational frequencies of the normal

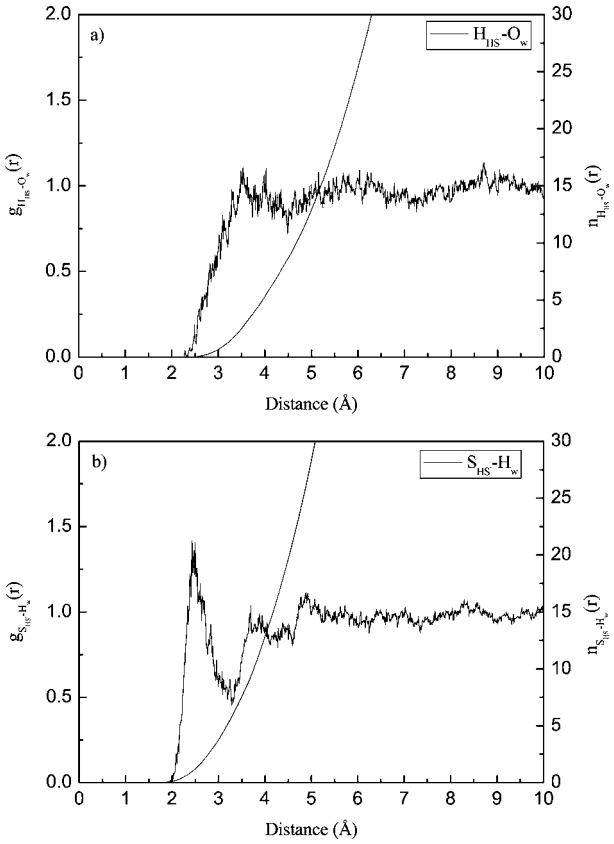

Figure 1. (a) $H_{HS^-}\cdots O_w$ and (b) $S_{HS^-}\cdots H_w$ RDFs and their corresponding integration numbers.

mode and the intermolecular $H_{HS^-}\cdots O_w$ interactions were calculated by their Fourier transformations of the velocity autocorrelation functions (VACFs). The normalized VACF, $C(t)$, is defined by

$$C(t) = \frac{\sum_{i}^{N_t}\sum_{j}^{N} v_j(t_i)\, v_j(t_i + t)}{N_t N \sum_{i}^{N_t}\sum_{j}^{N} v_j(t_i)\, v_j(t_i)} \qquad (7a)$$

where N is the number of particles, N_t is the number of time origins t_i, and v_j denotes a certain velocity component of the particle j. The power spectrum of $C(t)$ was determined using a correlation length of 2.0 ps.

3. Results and Discussion

3.1. Structural Properties. To describe the structural properties of the HS^- ion in aqueous solution, several hydration parameters such as radial distribution functions (RDF), coordination numbers, and angular distributions were determined. An averaged H−S bond distance of 1.35 Å was evaluated for HS^- in water. Figure 1 illustrates the radial distribution functions for both atoms of the HS^- ion and their neighboring water molecules together with the corresponding integration numbers. The first broad $H_{HS^-}\cdots O_w$ peak corresponding to the hydration shell is peaking ∼4 Å, covering a wide range of 2.1−4.6 Å. Weak intermediate peaks at 3.2 and 3.6 Å correspond to water molecules near the H of the HS^- ion. As the mean $H_{HS^-}\cdots O_w$ distance ∼4 Å is much larger than the $H_{HF}\cdots O_w$ and $H_{HCl}\cdots O_w$distances of 1.62 and 1.84 Å observed in aqueous HF and HCl solutions, respectively,[21,22] the extremely weak acidity of the H atom and thus its inability to form stable hydrogen bonds is clearly recognized. As visible in Figure 1a, the minimum between the first shell and bulk is far from the baseline, indicating frequent water exchanges and a very weak separation of the hydration shell from bulk. Figure 1b presents the $S_{HS^-}\cdots H_w$ RDF and the corresponding integration. The first sharp $S_{HS^-}\cdots H_w$ peak is centered at 2.42 Å, reflecting that the water molecules in the first hydration shell bind much more strongly to the sulfur site than to the hydrogen site. According to Figure 1b, a second $S_{HS^-}\cdots H_w$ peak within the range 3.2−4.0 Å with its maximum at ∼3.7 Å can be assigned to the distance between sulfur atom and the second hydrogen atom of coordinated water molecules in the hydration shell.

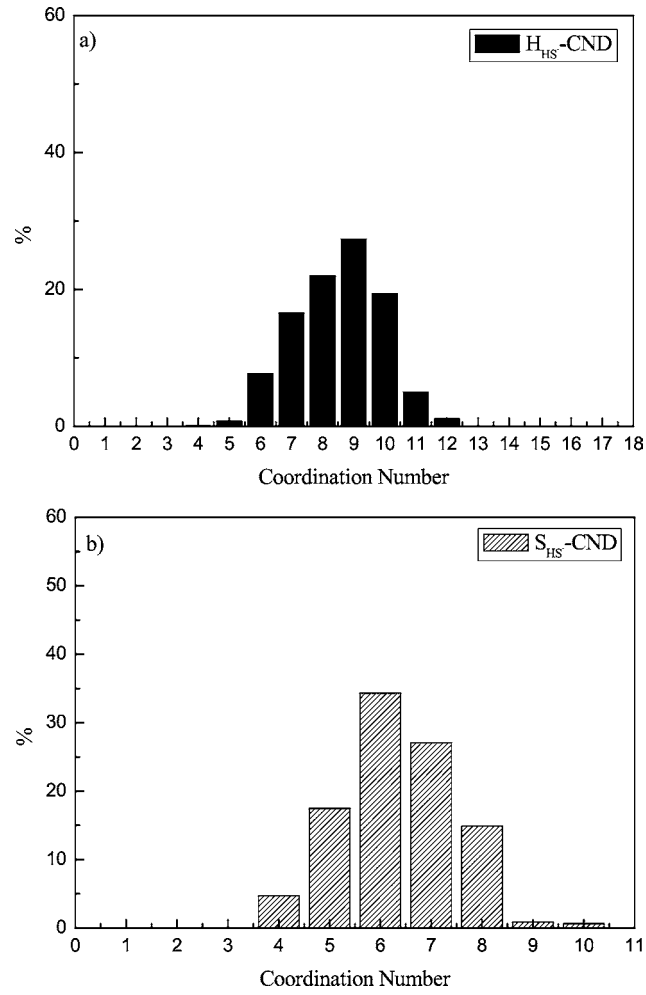

Figure 2. Coordination number distributions of (a) H (up to 4.5 Å) and (b) S (up to 4.0 Å) atoms in the first hydration shell of the HS^- ion.

The hydration shell coordination number distribution determined from the $H_{HS^-}\cdots O_w$ interactions of the HS^- ion in aqueous solution is shown in Figure 2a. A variation between 5 and 12, with 9 being the most dominant species is obtained from the simulation. As shown in Figure 2b, the coordination number distribution of the $S_{HS^-}\cdots O_w$ interactions covers a narrower range of 4−10 with an average value of 5.9 ± 1.1. These results confirm the assumption of a very weak water coordination at the hydrogen site of the HS^- ion. To see whether a true equilibrium has been established, the first and the second half of the sampling trajectory were analyzed separately and listed in Table 1. The results prove that there is only a minor

TABLE 1: Coordination Numbers for the Hydration Shell of the HS^- Ion Evaluated for Sulfur and Hydrogen Sites, and in a Molecular Manner

simulation time (ps)	CND-S	CND-H	CND-HS^-
0−5	5.9 ± 1.1	9.3 ± 1.6	10.2 ± 1.6
5−10	5.8 ± 1.0	9.0 ± 1.5	9.9 ± 1.5
0−10	5.9 ± 1.1	9.2 ± 1.6	10.0 ± 1.7

difference between both parts, which also gives a confidence limit for the overall results.

To further detail the hydrogen bond interactions of the HS^- ion in aqueous solution, the angular distribution functions of the $O_w\cdots H_{HS^-}-S_{HS^-}$ and $H_{HS^-}-S_{HS^-}\cdots H_w$ angles in the first hydration shell were examined as depicted in Figure 3. Both of these extend over almost the whole range from 0° to 180°, with a clear preference of nonlinear, almost rectangular H bonds. This result is in strong contrast to the cases of $O_w\cdots H-X$ bonds of HF (170°)[21] and HCl (161°).[22] The $H_{HS^-}-S_{HS^-}\cdots H_w$ angle peaking at ∼100° is smaller but not so different from the $H_{HF}-F_{HF}\cdots H_w$ and $H_{HCl}-Cl_{HCl}\cdots H_w$ angles of 116° and 112°.[21,22]

3.2. Dynamical Properties. On the basis of the velocity autocorrelation functions (VACFs) and their Fourier transformations, the vibrational frequencies of the normal mode $H_{HS^-}-S_{HS^-}$ and the intermolecular $H_{HS^-}\cdots O_w$ interactions were analyzed. The power spectra of the $H_{HS^-}\cdots O_w$ and $H_{HS^-}-S_{HS^-}$ vibrational modes of the hydrated ion obtained from the simulation are presented in Figure 4. As shown in Figure 4a, the maximum frequency of the $H_{HS^-}\cdots O_w$ vibrational mode in the first hydration shell is centered at 285 cm^{-1}, with two shoulder peaks at 204 and 383 cm^{-1}, corresponding to the force constants of 4.5, 2.3, and 8.2 N/m, respectively. The calculated force constant of 4.5 N/m obtained from the $H_{HS^-}\cdots O_w$ frequency is slightly weaker than the value of 5.9 N/m determined from the $H_{HF}\cdots O_w$ interaction.[21] However, it is much stronger than that of 1.6 N/m evaluated from the experimental $O_w-H_w\cdots O_w$ stretching frequency of 170 cm^{-1} in pure water.[39] This indicates a preference of the nondissociated structure of the HS^- ion, which was also observed in the case of HF.[21] The intramolecular $H_{HS^-}-S_{HS^-}$ stretching mode obtained from the QMCF MD simulation is centered at 2752 cm^{-1} (a value of 2449 cm^{-1} is obtained, if the intramolecular frequency is scaled by the standard factor of 0.89[40−42] for Hartree−Fock results), which is in reasonable agreement with the experimental evaluation by Raman spectroscopy (2570 cm^{-1}).[7] The deviation can be explained by the high concentration of perchlorate solution employed in the Raman study[7] and/or the inaccuracy of the Hartree−Fock method and the relatively small basis set. The force constant of 436.1 N/m for the $H_{HS^-}-S_{HS^-}$ bond confirms the stability of the HS^- ion in water.

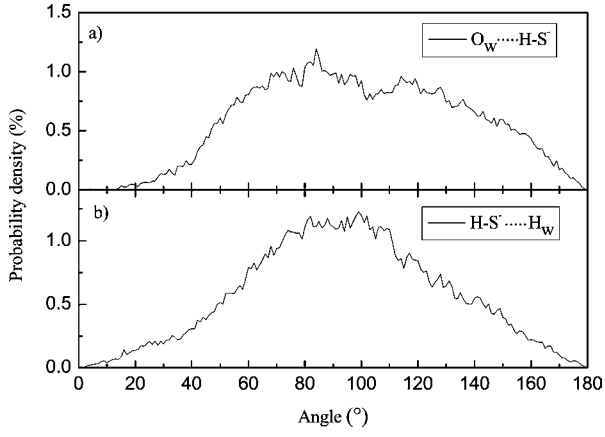

Figure 3. Distributions of (a) $O_w\cdots H_{HS^-}-S_{HS^-}$ angles and (b) $H_{HS^-}-S_{HS^-}\cdots H_w$ angles, obtained from the QMCF MD simulation.

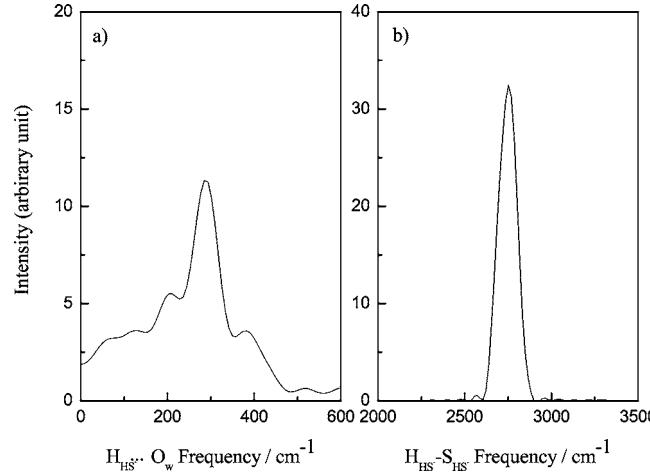

Figure 4. Power spectra of (a) $H_{HS^-}\cdots O_w$ and (b) $H_{HS^-}-S_{HS^-}$ stretching modes in the first hydration shell.

TABLE 2: Mean Ligand Residence Times and Sustainability of Migration Processes to and from the First Hydration Shell of Sulfur and Hydrogen atoms of the Bisulfide ion

		$t^* = 0$ ps		$t^* = 0.5$ ps		
solute	t_{sim}	N_{ex}^0	$\tau_{H_2O}^0$	$N_{ex}^{0.5}$	$\tau_{H_2O}^{0.5}$	R_{ex}
S_{HS^-}	10.0	190	0.3	40	1.5	4.8
H_{HS^-}	10.0	900	0.1	43	2.1	20.0
bulk[a]	10.0	131	0.2	20	1.3	6.5

[a] Values obtained from a QMCF MD simulation of pure water.[44]

Additional information about the solution dynamics was obtained in terms of the mean residence times (MRTs), corresponding to ligand exchange processes in the first hydration shell of the HS^- ion and determined by the "direct" method[43] for both sulfur and hydrogen sites of the HS^- ion. The number of ligand exchange processes, the mean residence times, and the number of attempts needed for a sustainable ligand migrating from the hydration shell as revealed by the use of both time parameters t^* 0.0 and 0.5 ps are listed in Table 2. As shown in Table 2, only 43 ligand exchange processes lasted longer than 0.5 ps at the hydrogen site of the HS^- ion during the simulation time of 10 ps, while 900 exchange attempts were recorded for $t^* = 0.0$ ps. The calculated MRT values for the hydrogen site are 0.1 ps and 2.1 for $t^* = 0.0$ and 0.5 ps, respectively. The MRT value of 2.1 ps is considerably larger than that of pure water determined from a QMCF simulation (1.3 ps)[44] and HCl (0.8 ps),[22] but it is slightly smaller than that of HF (2.5 ps).[21] At the sulfur site, the MRT values of 0.3 and 1.5 ps for $t^* = 0.0$ and 0.5 ps were obtained, corresponding to 190 and 40 exchange processes, respectively. As the result, the mean residence time for the water ligands located around the sulfur atom is shorter than that evaluated for the fluorine (2.1 ps) and chlorine (2.1 ps) sites of HF and HCl, respectively,[21,22] suggesting weak hydrogen bond interactions at the sulfur site of the HS^- ion. For the evaluation of hydrogen bond, the distances of 4.0 and 4.5 Å for hydrogen and oxygen atoms of water molecules and angle of >120° were applied to define hydrogen bonds between HS^- and water molecules. Hydrogen bond life times estimated for the $S_{HS^-}-H_{HS^-}\cdots O_w$ and $H_{HS^-}-S_{HS^-}\cdots H_w$ hydrogen bonds are 0.23 and 0.26 ps, respectively. The average

lifetime of the $S_{HS^-}-H_{HS^-}\cdots O_w$ hydrogen bond is much smaller than that determined by experimental investigation of pure water (0.55 ps),[45] and a QMCF MD simulation (0.33 ps).[44] The value of 0.26 ps of the $H_{HS^-}-S_{HS^-}\cdots H_w$ hydrogen bond is also smaller than the corresponding values of 0.36 and 0.31 ps for HF and HCl. These results reflect once more a very weak hydrogen bond between the HS^- ion and its neighboring water molecules in the hydration shell. According to the MRT values and the hydrogen bond lifetimes obtained from the QMCF MD simulation, the HS^- ion in aqueous solution behaves as weak structure-making species.

4. Conclusion

A detailed description on hydration structure and dynamics of the HS^- ion in aqueous solution could be obtained using a QMCF MD simulation. The $H_{HS^-}-S_{HS^-}$ vibrational frequency predicted from the QMCF MD simulation is in reasonable agreement with the experiment, while very weak hydrogen bonding between the bisulfide ion and its neighboring water molecules was recognized. These data confirm the preference of nondissociated HS^- in aqueous solution. As expected, ligand exchange processes in the hydration shell occur frequently at both sites of the HS^- ion.

Acknowledgment. Financial support for this work by the Thailand Research Fund (TRF) and Thailand Commission on Higher Education (ASEA-UNINET fellowships for C.K. and V.V.) are gratefully acknowledged and B.M.R. acknowledges support by the Austrian Science Foundation (FWF). V.V. acknowledges additional support by Faculty of Science, Chulalongkorn University (Grant Number RES A1 B1-19).

References and Notes

(1) Light, T. S. *Ion-Selective Electrodes*; National Bureau Standards Special Publication no. 314; NBS: Washington, DC, 1969; p 371.
(2) Wayne, R. P. *Chemistry of Atmospheres*, 2nd ed.; Clarendon Press: Oxford, U.K., 1991; *Chapters 1 and 5*.
(3) Barbero, J. A.; McCurdy, K. G.; Tremaine, P. R. *Can. J. Chem.* **1982**, *60*, 1872.
(4) Licht, S.; Manassen, J. *J. Electrochem. Soc.* **1987**, *134*, 918.
(5) Stephens, H. P.; Cobble, J. W. *Inorg. Chem.* **1971**, *10*, 619.
(6) Gigenbach, W. *Inorg. Chem.* **1971**, *10*, 1333.
(7) Meyer, B.; Ward, K.; Koshlap, K.; Peter, L. *Inorg. Chem.* **1983**, *22*, 2345.
(8) Licht, S.; Forouzan, F.; Longo, K. *Anal. Chem.* **1990**, *62*, 1356.
(9) Migdisov, A. A.; Williams, A. E.; Lakshtanov, L. Z.; Alekhin, Y. V. *Geochim. Cosmoschim. Acta* **2002**, *66*, 1713.
(10) Schoonen, M. A.; Barnes, H. L. *Geochim. Cosmoschim. Acta* **1988**, *52*, 649.
(11) Eckert, W. *J. Electrochem. Soc.* **1998**, *145*, 77.
(12) Kolthoff, L.; Moltzau, D. *Chem. Rev.* **1935**, *17*, 293.
(13) Luther, I., G. W.; Richard, D. T.; Theberge, S.; Olroyd, A. *Environ. Sci. Technol.* **1996**, *30*, 671.
(14) McCarthy, V. N.; Jordan, K. D. *Chem. Phys. Lett.* **2006**, *429*, 166.
(15) Joshi, R.; Ghanty, T. K.; Naumov, S.; Mukherjee, T. *J. Phys. Chem. A* **2007**, *111*, 2362.
(16) Lee, C.; Sosa, C.; Planas, M.; Novoa, J. *J. Chem. Phys.* **1996**, *104*, 7081.
(17) Planas, M.; Lee, C.; Novoa, J. J. *J. Phys. Chem.* **1996**, *100*, 16495.
(18) Smith, A.; Vencent, M. A.; Hillier, I. H. *J. Phys. Chem.* **1999**, *103*, 1132.
(19) Rode, B. M.; Hofer, T. S.; Randolf, B. R.; Schwenk, C. F.; Xenides, D.; Vchirawongkwin, V. *Theor. Chem. Acc.* **2006**, *115*, 77.
(20) Vchirawongkwin, V.; Pribil, A. B.; Rode, B. M. *J. Comput. Chem.* **2010**, *31*, 249.
(21) Kritayakornupong, C.; Vchirawongkwin, V.; Hofer, T. S.; Rode, B. M. *J. Phys. Chem. B* **2008**, *112*, 12032.
(22) Kritayakornupong, C.; Vchirawongkwin, V.; Rode, B. M. *J. Comput. Chem.* **2010**, *31*, 1785.
(23) Frick, R. J.; Hofer, T. S.; Pribil, A. B.; Randolf, B. R.; Rode, B. M. *J. Phys. Chem. A* **2009**, *113*, 12496.
(24) Hofer, T. S.; Pribil, A. B.; Randolf, B. R.; Rode, B. M. *Ab Initio Quantum Mechanical Charge Field Molecular Dynamics-A Nonparameterized First-Principle Approach to Liquids and Solutions*; Academic Press, Elsevier Inc.: Amsterdam, 2001; Vol. 59.
(25) Field, M. J.; Bash, P. A.; Karplus, M. *J. Comput. Chem.* **1990**, *11*, 700.
(26) Gao, J. *J. Am. Chem. Soc.* **1993**, *115*, 2930.
(27) Bakowies, D.; Thiel, W. *J. Phys. Chem.* **1996**, *100*, 10580.
(28) Stillinger, F. H.; Rahman, A. *J. Chem. Phys.* **1978**, *68*, 666.
(29) Bopp, P.; Janscó, G.; Heinzinger, K. *Chem. Phys. Lett.* **1983**, *98*, 129.
(30) Brooks, B. R.; Bruccoleri, R. E.; Olafson, B. D.; States, D. J.; Swaminathan, S.; Karplus, M. *J. Comput. Chem.* **1983**, *4*, 187.
(31) Berendsen, H. J. C.; Postma, J. P. M.; van Gunsteren, W. F.; DiNola, A.; Haak, J. R. *J. Chem. Phys.* **1984**, *81*, 3684.
(32) Adams, D. J.; Adams, E. H.; Hills, G. *J. Mol. Phys.* **1979**, *38*, 387.
(33) Ahlrichs, R.; Bär, M.; Häser, M.; Horn, H.; Kölmel, C. *Chem. Phys. Lett.* **1989**, *162*, 165.
(34) Ahlrichs, R.; von Arnim, M. *Methods and Techniques in Computational Chemistry: METECC-95*; Cagliari: Sardinia, 1995.
(35) von Arnim, M.; Ahlrichs, R. *J. Comput. Chem.* **1998**, *19*, 1746.
(36) Magnusson, E.; Schaefer, H. F., III. *J. Chem. Phys.* **1985**, *83*, 5721.
(37) Dunning, T. H., Jr.; Wadt, W. R. *J. Chem. Phys.* **1989**, *90*, 1007.
(38) Dunning, T. H., Jr.; Hay, P. J. *Modern Theoretical Chemistry: Methods of Electronic Structure Theory*; Schaefer, H. F., III, Ed.; Plenum Press: New York, 1977; Vol. 3.
(39) Franks, F. *Water: a Comprehensive Treatise*; Plenum Press: New York, 1972; *Vol. 1*.
(40) Scott, A. P.; Random, L. *J. Phys. Chem.* **1996**, *100*, 16502.
(41) Grev, R. S.; Janssen, C. L.; Schaefer, H. F., III. *J. Chem. Phys.* **1991**, *95*, 5128.
(42) DeFrees, D. J.; McLean, A. D. *J. Chem. Phys.* **1985**, *82*, 333.
(43) Hofer, T. S.; Tran, H. T.; Schwenk, C. F.; Rode, B. M. *J. Comput. Chem.* **2004**, *25*, 211.
(44) Randolf, B. R.; Hofer, T. S.; Rode, B. M. Unpublished results.
(45) Lock, A. J.; Woutersen, S.; Bakker, H. J. *J. Phys. Chem. A* **2001**, *105*, 1238.

JP104856Q

An *Ab Initio* Quantum Mechanical Charge Field Molecular Dynamics Simulation of a Dilute Aqueous HCl Solution

CHINAPONG KRITAYAKORNUPONG,[1] VIWAT VCHIRAWONGKWIN,[2] BERND M. RODE[3]
[1]*Faculty of Science, Department of Chemistry, King Mongkut's University of Technology, Thonburi, Bangkok 10140, Thailand*
[2]*Faculty of Science, Department of Chemistry, Chulalongkorn University, Bangkok 10330, Thailand*
[3]*Theoretical Chemistry Division, Institute of General, Inorganic and Theoretical Chemistry, University of Innsbruck, Innrain 52a, Innsbruck A-6020, Austria*

Received 19 June 2009; Revised 14 September 2009; Accepted 20 October 2009
DOI 10.1002/jcc.21469
Published online 17 December 2009 in Wiley InterScience (www.interscience.wiley.com).

Abstract: An *ab initio* quantum mechanical charge field (QMCF) molecular dynamics simulation has been performed to study the structural and dynamical properties of a dilute aqueous HCl solution. The solute molecule HCl and its surrounding water molecules were treated at Hartree-Fock level in conjunction with Dunning double-ζ plus polarization function basis sets. The simulation predicts an average H—Cl bond distance of 1.28 Å, which is in good agreement with the experimental value. The $H_{HCl}\cdots O_w$ and $Cl_{HCl}\cdots H_w$ distances of 1.84 and 3.51 Å were found for the first hydration shell. At the hydrogen site of HCl, a single water molecule is the most preferred coordination, whereas an average coordination number of 12 water molecules of the full first shell was observed for the chloride site. The hydrogen bonding at the hydrogen site of HCl is weakened by proton transfer reactions and an associated lability of ligand binding. Two proton transfer processes were observed in the QMCF MD simulation, demonstrating acid dissociation of HCl. A weak structure-making/breaking effect of HCl in water is recognized from the mean residence times of 2.1 and 0.8 ps for ligands in the neighborhood of Cl and H sites of HCl, respectively.

 J Comput Chem 31: 1785–1792, 2010

Key words: hydrogen chloride; hydration structure; dynamical properties; hydrogen bond; acid dissociation; proton transfer; simulation; QMCF

Introduction

It is well known that hydrogen bond formation and proton transfer of hydrogen halides in aqueous solution play an important role in a wide range of chemical and biological processes.[1] Hydrogen chloride is a strong acid with $pK_a = -7$, indicating a dissociated form of hydrogen chloride in dilute aqueous solution. There are very few experiments related to the hydration structure of HCl in aqueous solution.[2–6] Matrix isolation spectroscopy of $HCl(H_2O)_n$ complexes was performed, showing the nondissociated structure of HCl with $n \leq 3$, whereas proton transfer is achieved from the complex with $n = 4$.[2] X-ray and neutron diffraction techniques were applied to evaluate the structure of the aqueous HCl acid solution at 20°C and it was found that four water molecules were required to solvate each hydronium and Cl^- ions in solution.[3] Concentrated HCl solutions were also studied using spectroscopic and diffraction techniques, suggesting a pentagonal ring structures of $HCl(H_2O)_6$ and $(HCl)_2(H_2O)_6$ in solution.[4] Ragout-jet Fourier transform infrared spectroscopy was used to evaluate the proton vibrational dynamics in $(HCl)_m$–$(H_2O)_n$ clusters, reporting that HCl complexes with three or more water molecules could not be assigned in the IR spectrum.[5] Recently, X-ray absorption of aqueous HCl solution was investigated. It was found that the addition of HCl to liquid water leads to a decrease in intensity of the X-ray absorption spectrum.[6] In addition, neutron diffraction of a highly concentrated HCl solution has been performed to determine the Eigen or Zundel complexes, but its results are not comparable to the species formation in dilute HCl solution.[7] Numerous theoretical techniques have been applied to describe the characteristics of

Correspondence to: C. Kritayakornupong; e-mail: chinapong.kri@kmutt.ac.th

Contract/grant sponsors: Thailand Research Fund (TRF), Thailand Commission on Higher Education, Austrian Science Foundation (FWF)

HCl in aqueous solution.[4–6,8–25] An MP2/6-31+G* calculation in the continuum model of water confirmed the nondissociation of monohydrated and dihydrated HCl complexes.[8] HCl on an ice surface at 190 K was studied using molecular dynamics simulations, indicating that ionic solvation processes are thermodynamically feasible.[9,10] A calculation using BLYP level of approximation with an extended basis set showed that the proton transfer takes place without transition state in the case of $HCl(H_2O)_4$.[11] Using the MP2 method, a nondissociated HCl complex was observed with a cyclic three-water cluster, indicating a red-shift in the HCl stretching frequency,[13] whereas the dissociated form appears to be possible when the HCl molecule was surrounded by four water molecules.[15] The MP2/6-311++G(d,p) level of theory was applied to describe the nondissociated form of HCl with four water molecules.[18] Upon extension of the cluster size to five water molecules, proton transferred type was shown to exist. The nondissociated form was determined as the most stable structure for the $HCl(H_2O)_n$ ($n = 1 - 3$) clusters evaluated by the B3LYP/D95++(d,p) method.[19] The $HCl(H_2O)_4$ cluster resulted as an intermediate with both nondissociated and dissociated structures obtained from both the B3LYP and the MP2 method.[19,22] Car-Parrinello molecular dynamics (CPMD) simulations were performed to evaluate the dissociation and vibrational dynamics of DCl in D_2O molecules.[12,16,23–25] Concentrated HCl solutions (2.7 and 5.3 M) where complete dissociation has already been assumed by the composition of the system (protons, Cl^- ions, and water) have also been studied by CPMD simulations,[26] in which the gradient-corrected BLYP functional has been used that usually leads to too rigid H-bonds and thus to too slow dynamics. The amount of solvent considered further does not provide sufficient water molecules for a full hydration of ions. Monte Carlo simulations were applied to investigate the mechanism of HCl ionization in water.[17,20] Furthermore, the vibrational spectra of aqueous HCl were evaluated in both experimental and theoretical studies.[4,5,13,19–25] The results obtained thereby showed that the number of water molecules surrounding HCl and the accuracy of approximation methods utilized play a significant role on characteristics and stability of proton transferred and proton nontransferred HCl forms in aqueous solution. Summarizing all of these results, therefore, our intentions were (i) To investigate HCl in very dilute aqueous solution, providing the possibility of full hydration (498 water molecules for one HCl molecule). (ii) To utilize an *ab initio* HF method in an extended QM region with the new quantum mechanical charge field (QMCF) methodology. HF is known to lead to slightly too weak H-bonds, but proved more suitable than DFT in many systems.[27,28] (iii) To start with undissociated HCl to see, whether dissociation would occur readily.

To answer these questions, in this study, we have performed an *ab initio* QMCF molecular dynamics simulation of HCl in aqueous solution. The structure of aqueous HCl solution was evaluated in terms of radial distribution functions, coordination numbers, angular distributions, θ-angle, and tilt angle distributions. To describe the dynamical properties, the mean ligand residence times for ligand exchange processes between hydration shell of HCl and bulk and the vibrational frequency of H—Cl were also determined.

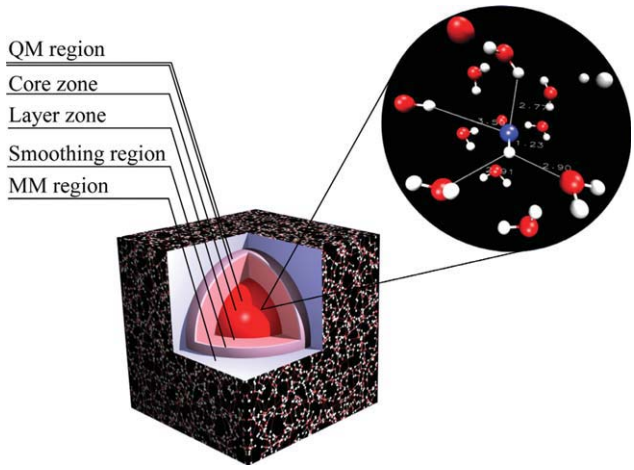

Figure 1. Definition of the quantum mechanical (QM) and molecular mechanical (MM) regions in the QMCF approach.

QMCF MD Simulation

The *ab initio* QMCF molecular dynamics technique[29] is similar to conventional QM/MM MD methods[30–32] in which the system is separated into two regions, namely QM and MM regions. In the QMCF method, the QM region is enlarged to include the second hydration shell and consists of two subregions, the so-called "core region" (inner QM subregion) and the "layer region" (outer QM subregion), as shown in Figure 1. By using the QMCF method, no solute–solvent potentials are required, and an improved handling of Coulombic interactions is introduced. The calculated forces between the core region and the MM region are the major difference between the QM/MM MD and the QMCF MD simulation. In the QMCF MD simulation, the forces acting on each particle in the different regions are defined as

$$F_j^{\text{core}} = F_j^{\text{QM}} + \sum_{i=1}^{M} \frac{q_j^{\text{QM}} q_i^{\text{MM}}}{r_{ij}^2} \tag{1}$$

$$F_j^{\text{layer}} = F_j^{\text{QM}} + \sum_{i=1}^{M} \frac{q_j^{\text{QM}} q_i^{\text{MM}}}{r_{ij}^2} + \sum_{i=1}^{M} F_{ij}^{\text{BJHnC}} \tag{2}$$

$$F_j^{\text{MM}} = \sum_{\substack{i=1 \\ i \neq j}}^{M} F_{ij}^{\text{BJH}} + \sum_{i=1}^{N_1+N_2} \frac{q_i^{\text{QM}} \cdot q_j^{\text{MM}}}{r_{ij}^2} + \sum_{i=1}^{N_2} F_{ij}^{\text{BJHnC}} \tag{3}$$

where F_j^{core} is the quantum mechanical force acting on the particle j in the core region, F_j^{layer} is the forces acting on particle j located in the solvation layer, F_j^{MM} represents the forces acting on the particle j in the MM region, and M is the number of atoms in the MM region. In each simulation step, the forces in the core and layer region (F_j^{core}, F_j^{layer}) are calculated from the *ab initio* quantum mechanical treatment plus the Coulombic forces obtained from all MM atoms, whereas the forces in the

MM region (F_j^{MM}) are obtained from the BJH-CF2 water model[33,34] augmented by the Coulombic forces exerted by all atoms in the core region (N_1) and the layer region (N_2), and the noncoulombic forces generated by the atoms in the layer region (N_2). Consequently, the QM forces in the layer (F_j^{layer}) are supplemented by the noncoulombic forces of particles in the MM region evaluated from the BJH-CF2 water model.[33,34] The Coulombic interactions are calculated with the point charges of the atoms in the MM region and the quantum chemically evaluated partial charges on the atoms in the QM region. The charges of the particles in the MM region are incorporated via a perturbation term into the core Hamiltonian:

$$H_{CF} = H_{HF} + V_i'$$

$$V_i' = \sum_{j=1}^{M} \frac{q_j}{r_{ij}} \tag{4}$$

where q_j are the partial charges of each MM atoms obtained by Mulliken population analysis, which proved to be best compatible with the BJH-CF2 water model. The oxygen and hydrogen charges are -0.65996 and $+0.32983$, according to the charges of the BJH-CF2 water model utilized in the MM region.[33,34]

In the QMCF MD simulation, solvent molecules can freely migrate between the QM and MM region. A smoothing function[35] is applied between the radii r_0 (5.7 Å) and r_1 (5.5 Å), corresponding to an interval of 0.2 Å, to ensure a continuous transition of forces at the boundary. The forces acting on each particle in the system can be defined as:

$$F_j^{Smooth} = F_j^{MM} + (F_j^{layer} - F_j^{MM}) \cdot S_m(r) \tag{5}$$

where F_j^{MM} represents the force acting on the particle j in the MM region, F_j^{layer} is the force acting on the particle j located in the solvation layer, r is the distance of the water molecule from the chlorine atom of the solute molecule, and S_m a smoothing function.[35]

$$\begin{aligned} S_m(r) &= 1, && \text{for } r \le r_1 \\ S_m(r) &= \frac{\left(r_0^2 - r^2\right)^2 \left(r_0^2 + 2r^2 - 3r_1^2\right)}{\left(r_0^2 - r_1^2\right)^3}, && \text{for } r_1 < r \le r_0 \\ S_m(r) &= 0, && \text{for } r > r_0, \end{aligned} \tag{6}$$

where r_1 is the inner border of the smoothing region and r_0 is the radius of the QM region. Further details of this method are given in ref. 31.

This simulation protocol used in the present work is similar to that applied in a previous simulation of aqueous HF solution[36] and has been successfully applied to investigate characteristics of several composite chemical species in solution.[29,36–39] The QMCF MD simulation was performed in a periodic boundary cubic box with a side length of 24.65 Å, containing one hydrogen chloride molecule plus 498 water molecules. Temperature was controlled by the Berendsen temperature-scaling algorithm[40] with a relaxation time of 100 fs to maintain 298.15 K. The density of the simulation was fixed at 0.997 g/cm^3, corresponding to the experimental value of pure water. A predictor–corrector algorithm was used to integrate the Newtonian equations of motion with the chosen time step of 0.2 fs. The flexible BJH-CF2 water model[33,34] including an intramolecular potential was used to elucidate the interactions between pairs of water molecules in the MM region, as it allows explicit hydrogen movements, and thus, also a smooth transition of water molecules from the QM to the MM region and vice versa. The reaction field[41] was applied to correct for long-range Coulombic interactions. Cutoff distances of 5 and 3 Å were used for noncoulombic O—H and H—H interactions, respectively. The radial cutoff limit for Coulombic interactions was set to half the box length. The values of 6.0 and 11.0 Å were chosen for the diameters of the core and the layer region, respectively, and hence, the full first hydration shell and a part of the second hydration shell are included in the QM region, according to the radial distribution functions (RDF) in the equilibrated state. The TURBOMOLE 5.9 program[42–44] was used to evaluate the forces in the QM region calculated at the restricted Hartree-Fock level. Dunning double-ζ plus polarization function (DZP) basis sets[45,46] were applied for chlorine, oxygen, and hydrogen atoms. These basis sets were chosen as a suitable compromise between accuracy of the results and computational effort. Many test calculations with the DZP basis sets comparing solvent clusters with one to six water molecules by HF, B3LYP, MP2, and CSSD have shown that the error by neglecting electron correlation is very minor.[47–50] Moreover, the QM/MM simulation using the B3LYP functional have revealed deviating descriptions such as too rigid structures for solvates and H-bonded systems.[51–53] In addition, the influence of the basis set super position error (BSSE) for HCl monohydrate was also determined at several levels of theory. The lowest BSSE energy of 0.2 kcal/mol was obtained from the HF method, whereas the values of 0.5, 0.9, and 0.8 kcal/mol were evaluated from the B3LYP, MP2, and CCSD methods, respectively. These indicate that the effects of electron correlation and BSSE should have only a minor influence on quality of the QMCF simulation results. The QMCF MD simulation was equilibrated for 2 ps and total of 10 ps was performed for sampling. Simulation time had to be limited to 50,000 steps of 0.2 fs (needed to appropriately describe hydrogen movements) as these 10 ps already consume 5 months of CPU time on a 4 AMD Opteron 2.8 GHz processors high performance computer.

Velocity autocorrelation functions (VACFs) were used to determine the dynamical properties of HCl in aqueous solution. With $C_{\infty v}$ symmetry of the HCl molecule, the vibrational motion of the HCl molecule is both infrared active and Raman active. The velocities of the hydrogen atom of HCl and the oxygen atom of H_2O were projected onto a unit vector parallel to the corresponding Cl—H bond ($\vec{\mathbf{u}}_1$) and $H_{HCl}\cdots O_w$ direction ($\vec{\mathbf{u}}_2$), respectively, thus the vibrational modes are the projections of the hydrogen and oxygen velocities onto the unit vectors $\vec{\mathbf{u}}_1$ and $\vec{\mathbf{u}}_2$, respectively. The vibrational frequencies of the normal mode and the intermolecular $H_{HCl}\cdots O_w$ interactions were calculated by their Fourier transformations of the VACFs. The normalized VACF, $C(t)$, is defined by

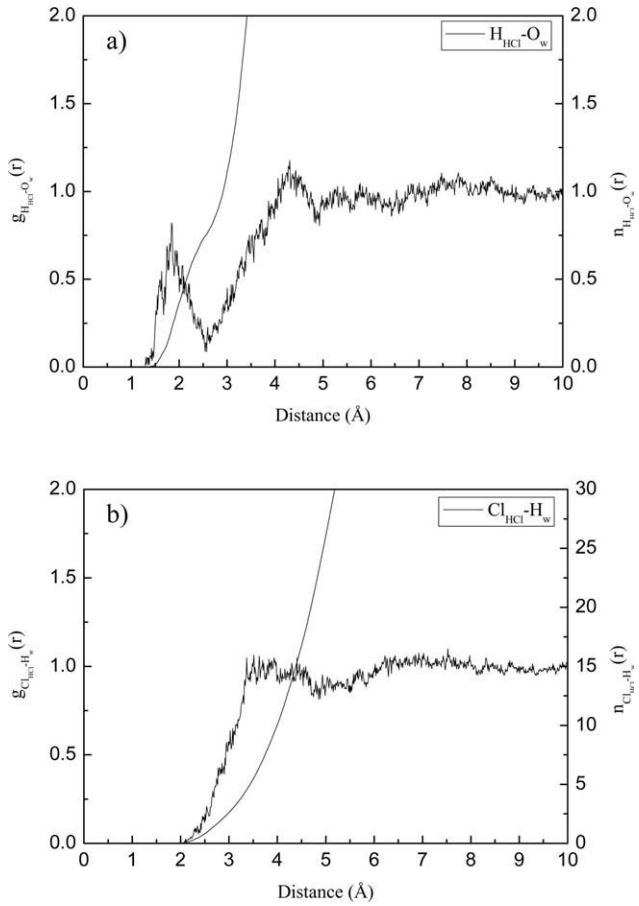

Figure 2. (a) $H_{HCl}\cdots O_w$, and (b) $Cl_{HCl}\cdots H_w$ RDFs and their corresponding integration numbers.

$$C(t) = \frac{\sum_i^{N_t} \sum_j^N v_j(t_i) v_j(t_i + t)}{N_t N \sum_i^{N_t} \sum_j^N v_j(t_i) v_j(t_i)}, \quad (7)$$

where N is the number of particles, N_t is the number of time origins t_i, and v_j denotes a certain velocity component of the particle j.

Results and Discussion

Structural Properties

The hydration structure of the HCl in aqueous solution was evaluated in terms of RDF, coordination numbers, and angular distributions. In the QMCF MD simulation, The H—Cl distance varies in the range of 1.2–1.5 Å, with an averaged value of 1.28 Å, which is in good agreement with the experimental value of 1.274 Å.[54,55] Figure 2 shows the radial distribution functions for each atom of HCl and its neighboring water molecules together with their corresponding integration numbers evaluated from the QMCF MD simulation. The first peak in the $H_{HCl}\cdots O_w$ RDF characterizes the first hydration shell, located between 1.5 and 2.5 Å with a maximum value of 1.84 Å. This value is larger than that determined in the case of an aqueous HF solution (1.62 Å).[36] The second peak corresponding to the water ligands near the Cl atom in the first hydration shell is located at 4.30 Å. The $Cl_{HCl}\cdots H_w$ RDF and the corresponding integration are depicted in Figure 2b. The first $Cl_{HCl}\cdots H_w$ peak lies within the range of 2.0–4.0 Å, showing its maximum at 3.51 Å with additional peaks at 3.36, 3.62, and 3.93 Å. The $Cl_{HCl}\cdots H_w$ second peak is situated at 4.40 Å, covering distances of 4.0–4.7 Å, and corresponds to the second H atom of coordinated water molecules.

The coordination number distributions of the first hydration shell determined from the $H_{HCl}\cdots O_w$ and $Cl_{HCl}\cdots O_w$ interactions of the aqueous HCl solution are displayed in Figure 3. According to Figure 3a, a single water molecule bound to the H site of the HCl molecule is the most dominant coordination with 74%

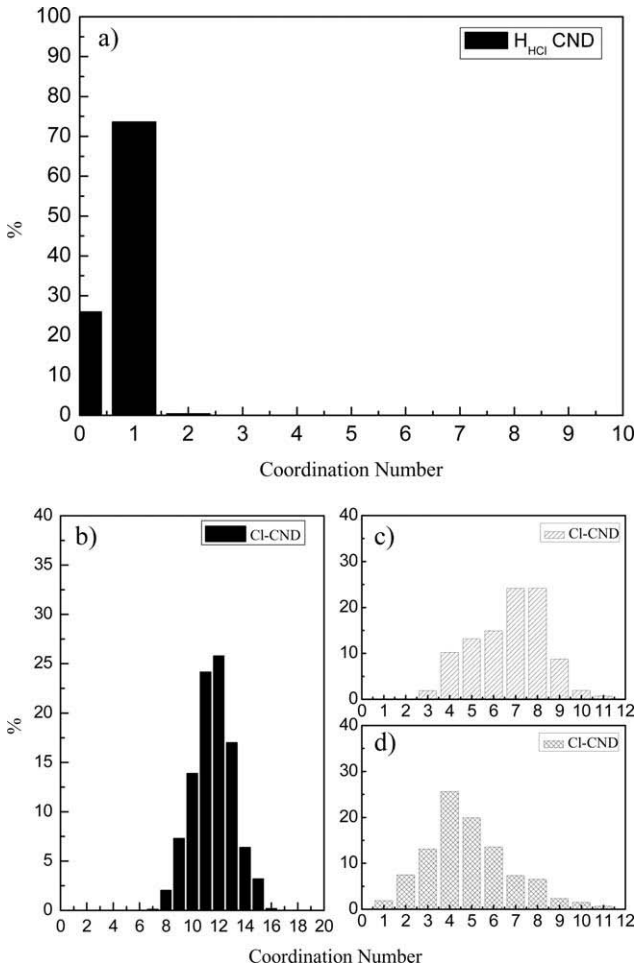

Figure 3. Coordination number distributions of (a) H and (b) Cl atoms in the first hydration shell of HCl, (c) Cl atom in immediate first shell from 0.0 to 4.2 Å, and (d) Cl atom in extended first hydration shell from 4.2 to 4.8 Å.

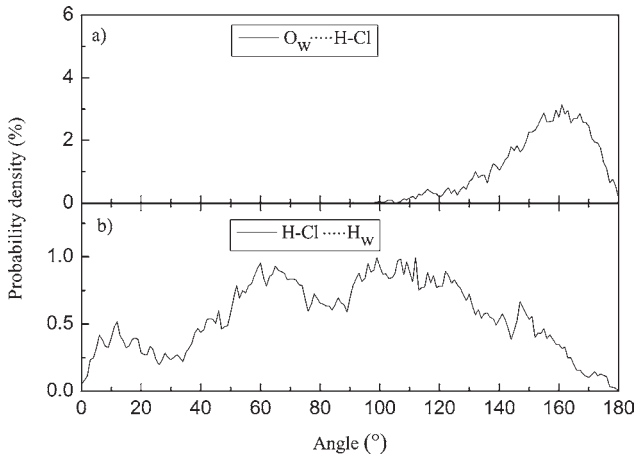

Figure 4. Distributions of (a) $O_w\cdots H_{HCl}—Cl_{HCl}$ angles and (b) $H_{HCl}—Cl_{HCl}\cdots H_w$ angles, obtained from the QMCF MD simulation.

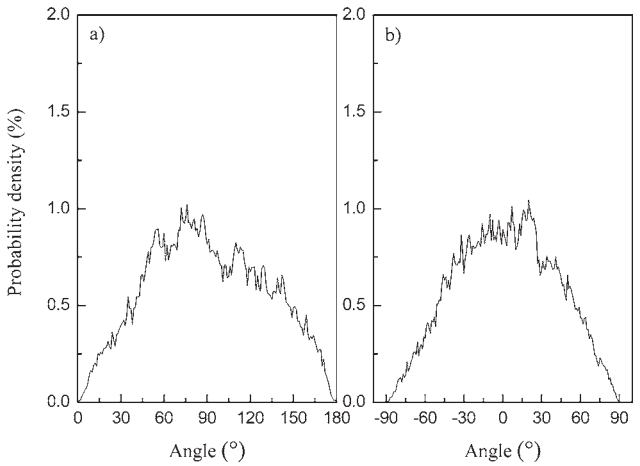

Figure 5. The θ and tilt angular distributions of water ligands near the HCl molecule.

occurrence. The $Cl_{HCl}\cdots O_w$ RDF displays two distinguished parts of the first hydration shell, one representing an extended first hydration shell located between 4.2 and 4.8 Å. Therefore, the coordination number distributions of the water molecules in the substructure near the Cl atom were examined and depicted in Figures 3b–3d. As shown in Figure 3c, the coordination number distribution integrated up to the distance of 4.2 Å of the first part of the $Cl_{HCl}\cdots O_w$ peak covers a wide range of 3–11, giving an average value of 6.7. For the extended first hydration shell, an average coordination number of 4.9 was found with a large variation in the hydration numbers ranging from 1 to 11. These findings indicate almost seven water molecules to be directly bound to the Cl site of the HCl molecule, while in average five water molecules are located in the extended first hydration shell. This shows that the frequent ligand exchange processes must occur at the Cl site, whereas the one water molecule bound to the H atom seems to be more stably coordinated.

The hydrogen bond angle between HCl and water molecule can be determined in terms of the angular distribution functions of the $O_w\cdots H_{HCl}—Cl_{HCl}$ and $H_{HCl}—Cl_{HCl}\cdots H_w$ angles in the first hydration shell. According to Figure 4a the $O_w\cdots H_{HCl}—Cl_{HCl}$ angular distribution has its maximum at 161° with tailing until 100°, proving the preference for linear $O_w\cdots H_{HCl}—Cl_{HCl}$ hydrogen bond arrangements. However, considerably less linearity of this hydrogen bond in the case of HCl was observed in comparison with HF, where the $O_w\cdots H_{HF}—F_{HF}$ angular distribution is situated at 170° with variation down to 100°.[36] The presence of nonlinear, weak, and flexible hydrogen bonds between water and the Cl site of HCl is recognized from three dominant $H_{HCl}—Cl_{HCl}\cdots H_w$ peaks at 12°, 60°, and 112°, respectively. The low angle value of 12° reflects the arrangement of two hydrogen bonds in the intermediate HCl monohydrate ($Cl_{HCl}\cdots H_w$ and $H_{HCl}\cdots O_w$).

To further characterize the flexibility and orientation of the water molecules surrounding HCl in the first hydration shell, angle θ and tilt angle are introduced. The angle θ is the angle between the vector pointing along $C_g—O_w$ (C_g is the center of mass of the HCl molecule) and the dipole vector of water molecule. The tilt angle is the angle between the $H_{HCl}—Cl_{HCl}$ axis and the plane defined by the $O_w—H_w$ vectors. Figure 5 presents the θ and tilt angular distributions in the first hydration shell of HCl. The broad peak of the angle θ distribution obtained from the QMCF MD simulation has its maximum at 76°, covering a wide range of 0–180°. A similar result was also observed in the case of HF.[36] However, the maximum value of 136° evaluated for HF is much larger than that determined from HCl. The maximum value of the tilt angle for the first shell is located at 20°, and the distribution reaches 0 at ±90°. Both angle distributions prove a very high flexibility of the first shell ligands' orientation.

Dynamical Properties

The vibrational frequencies of the normal mode $H_{HCl}—Cl_{HCl}$ and the intermolecular $H_{HCl}\cdots O_w$ interactions were examined using the VACFs and their Fourier transformations. Figure 6

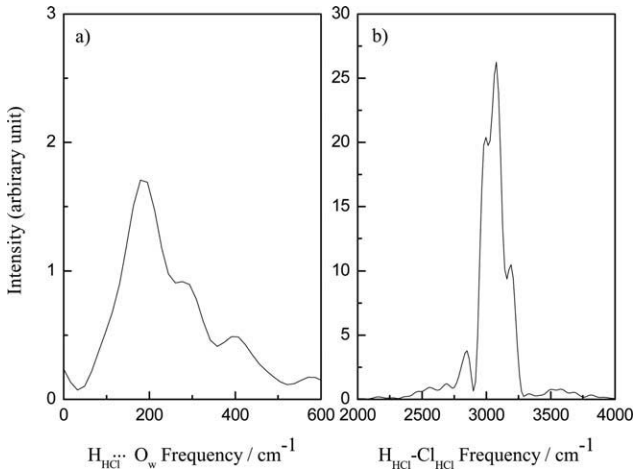

Figure 6. Power spectra of (a) $H_{HCl}\cdots O_w$ and (b) $H_{HCl}—Cl_{HCl}$ stretching modes in the first hydration shell.

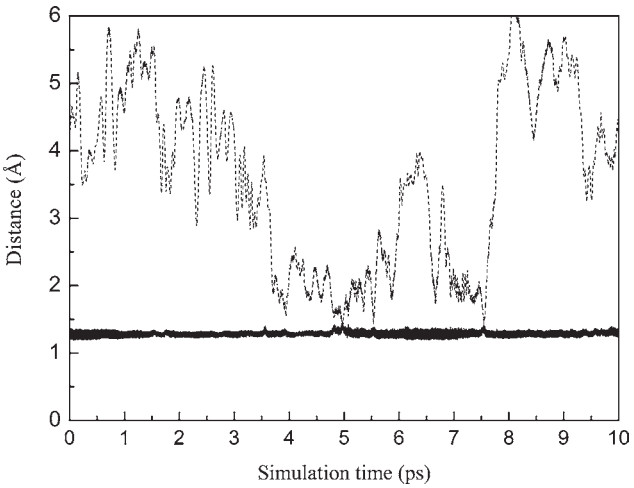

Figure 7. The $H_{HCl}\cdots Cl_{HCl}$ (solid line) and $H_{HCl}\cdots O_w$ (dashed line) distances as a function of time in the first hydration shell evaluated for the proton transfer processes.

illustrates the power spectra of the $H_{HCl}\cdots O_w$ and $H_{HCl}—Cl_{HCl}$ vibrational motions in the first hydration shell obtained from the QMCF MD simulation. In Figure 6a, the maximum frequency of the $H_{HCl}\cdots O_w$ vibrational mode in the first hydration shell is situated at 179 cm^{-1}, with two shoulder peaks at 277 and 390 cm^{-1}. The force constant of 1.8 N/m was calculated for this frequency of the $H_{HCl}\cdots O_w$ peak, which is much weaker than that obtained for the $H_{HF}\cdots O_w$ interaction (5.9 N/m),[36] but slightly stronger than the value of 1.6 N/m retrieved from the experimental $O_w—H_w\cdots O_w$ stretching (170 cm^{-1}).[56] This demonstrates that the acid dissociation of HCl is much more facilitated than that of HF, since the $H_{HCl}\cdots O_w$ hydrogen bond interaction is almost equally weak as the $O_w—H_w\cdots O_w$ interaction in pure water. For the $H_{HCl}—Cl_{HCl}$ stretching motion, the highest value of this mode is centered at 3078 cm^{-1}, with two shoulder peaks at 2997 and 3192 cm^{-1}. The force constants evaluated for these peaks are 547.1, 518.7, and 588.4 N/m, respectively. The $H_{HCl}—Cl_{HCl}$ stretching frequency calculated from the QMCF simulation is in reasonable agreement with the experimental harmonic vibrational frequency of 2990 cm^{-1}.[57,58] In addition, the gas-phase value of 3153 cm^{-1} for the $H_{HCl}—Cl_{HCl}$ stretching frequency was also evaluated from the HF/DZP method to confirm that this agreement is not a coincidence. The value of 547.1 N/m estimated for the force constant in the case of HCl is much weaker than that observed for HF (819.1 N/m),[36] proving less stability of the nondissociated form of HCl. It was further found that the ligand exchange processes in the H site of HCl causes the shoulder peaks in the $H_{HCl}—Cl_{HCl}$ stretching mode.

Table 1. The Energy Parameters for the $HCl(H_2O)_4$ Clusters Calculated by Different Levels of Theory.

Method	$HCl(H_2O)_4$ undissociated form (Hartree)	$HCl(H_2O)_4$ dissociated form (Hartree)	ΔE (kcal/mol)[a]
HF/DZP	−764.2932329	−764.2869273	3.96
BLYP/DZP[b]	–	−766.5469201	–
B3LYP/DZP[b]	–	−766.6512601	–
MP2/DZP	−765.2326384	−765.2291570	2.18
CCSD/DZP	−765.2784585	−765.2715970	4.31

[a]The relative energies of the dissociated form with that of the undissociated form.
[b]Only the dissociated forms were observed.

Table 2. Mean Ligand Residence Times and Sustainability of Migration Processes to and from the First Hydration Shell of Chlorine and Hydrogen Atoms of the Hydrogen Chloride Molecule.

		$t^* = 0$ ps		$t^* = 0.5$ ps			
Solute	t_{sim}	N_{ex}^0	$\tau_{H_2O}^0$	$N_{ex}^{0.5}$	$\tau_{H_2O}^{0.5}$	S_{ex}	$1/S_{ex}$
Cl_{HCl}	10.0	392	0.3	56	2.1	0.14	7.1
H_{HCl}	10.0	80	0.1	9	0.8	0.11	9.1
Bulk[a]	10.0	269	0.2	24	1.7	0.09	11.2

[a]Values obtained from a QM/MM MD simulation of pure water.[52]

To characterize the acid dissociation of HCl, the ionization structure of this acid has been evaluated. Figure 7 shows distributions of the $H_{HCl}\cdots Cl_{HCl}$ and $H_{HCl}\cdots O_w$ distances in the first hydration shell, exhibiting the proton migration from the chlorine atom of hydrogen chloride to oxygen of a neighboring water. The first proton migration takes place around 4.9–5.0 ps and the second one occurs during the simulation time of 7.5–7.6 ps. Another dissociation attempt observed at 5.5 ps is not completed, but almost successful. It is seen that the proton coming from HCl bound to the neighboring water forming H_3O^+ species comes back to the Cl atom reforming the HCl molecule within the femtosecond scale. Despite the short simulation time of 10 ps, three proton migration processes were observed, which shows that dissociation can occur already on the picosecond scale in very dilute solution. In the previous CPMD simulation,[16] corresponding to a higher concentration, a number of

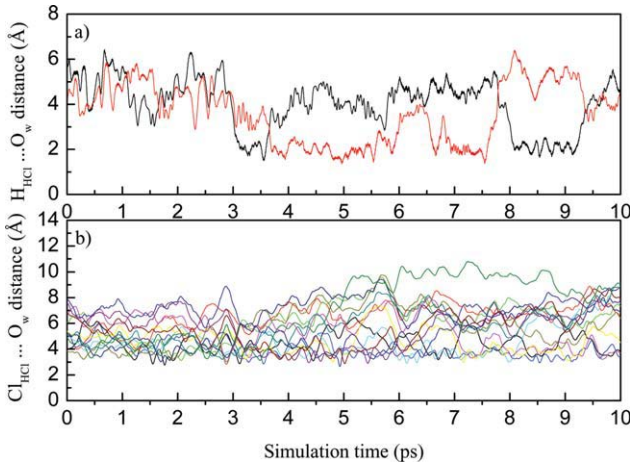

Figure 8. (a) The $H_{HCl}\cdots O_w$ and (b) the $Cl_{HCl}\cdots O_w$ distances as a function of time in the first hydration shell obtained from the QMCF MD simulation.

error sources can be identified, partly due to the early time it has been performed, such as the use of DCl and D_2O and the functionals being used, for which several problems have been identified in the meantime.[59] As previous cluster calculations (DFT and MP2)[19,22] have already shown that DFT overrates the stability of the dissociated state, it seemed appropriate to perform new cluster calculations including HF, MP2, CCSD, and the more modern B3LYP density functional, and the results, shown in Table 1, clearly prove that DFT leads to an unjustified preference for the dissociated state. It should be emphasized, however, that the frequent attempts of proton transfer in our simulation within a few picoseconds are a clear indication that over a longer time period a number of them will be successful thus creating a sufficient number of hydronium ions. For study of full dissociation, i.e., separation of Cl^- and hydrated hydronium ion, a longer simulation time would have been required but on the basis of the results obtained for 10 ps one can easily predict such a dissociation process to happen.

The dynamics of ligand exchange processes at each atom of HCl were also determined by the mean residence times (MRTs) using the "direct" method.[60] The time parameters t^* of 0.0 and 0.5 ps were used, reflecting to the minimum duration of a ligand's displacement from its original coordination shell to be accounted. The number of ligand exchange processes, the MRTs, and the sustainability of migration processes from the first hydration shell are summarized in Table 2. The variations of the $H_{HCl}\cdots O_w$ and $Cl_{HCl}\cdots O_w$ distances obtained at $t^* = 0.5$ ps in the first hydration shell are presented in Figure 8. As shown in Figure 8a, there are three exchange processes occurring at the H atom of HCl, the first one taking place at 3.5 ps and the second and the third one observed in the range of 6–7 and 7–8 ps, respectively. For the Cl site, several ligand exchange processes were found during the simulation time of 10 ps, as shown in Figure 8b. The calculated MRT values with respect to $t^* = 0.0$ and 0.5 ps for the first hydration shell located around the Cl atom are 0.3 and 2.1 ps, which are the same as those estimated for the F site of HF.[36] The values of 0.1 and 0.8 ps for $t^* = 0.0$ ps and $t^* = 0.5$ ps, respectively, were determined for the H site of HCl. These values are smaller in comparison with the aqueous HF solution (0.8 ps for $t^* = 0.0$ ps and 2.5 ps for $t^* = 0.5$ ps),[36] and also smaller than that obtained from QM/MM (1.51 ps)[53] simulation of pure water. In the QMCF MD, hydrogen bond life times of 1.1 and 0.31 ps were evaluated for the $Cl_{HCl}—H_{HCl}\cdots O_w$ and $H_{HCl}—Cl_{HCl}\cdots H_w$ hydrogen bonds, respectively, suggesting a very different stability of these H-bonds. The average lifetime of the $Cl_{HCl}—H_{HCl}\cdots O_w$ hydrogen bond is higher than that observed in pure water by experiment[61] (0.55 ps), and a QM/MM MD simulation (0.33 ps),[53] confirming the stability of this H bond. The value of 0.31 ps obtained for the $H_{HCl}—Cl_{HCl}\cdots H_w$ hydrogen bond is almost the same as the value of 0.36 determined for the F site of the HF molecule. The MRT values and the hydrogen bond lifetimes predicted from the QMCF MD simulation reveal that HCl in aqueous solution is simultaneously a weak structure-making and a weak structure breaking species. The sustainability coefficients S_{ex} were computed by comparing the number of all exchanges through the border of the hydration shell ($N_{ex}^{0.0}$) to the number of exchanges processes lasting at least 0.5 ps ($N_{ex}^{0.5}$), resulting in 0.11 and 0.14 for H and Cl sites of hydrogen chloride. The corresponding $1/S_{ex}$ values are 9.1 and 7.1, suggesting that one lasting exchange process in the neighborhood of H and Cl is achieved by about nine and seven attempts to cross a shell boundary, respectively.

Conclusions

We have performed a QMCF molecular dynamics simulation to investigate the hydration structure and dynamics of the aqueous HCl solution. The calculated H—Cl bond distance and its vibrational frequency are in good agreement with the experimental observation. A relatively strong hydrogen bond at the H site of hydrogen chloride was detected, whereas weak hydrogen bonding dominates at the Cl site. The coordination number of ~7 is prevailing in the first hydration shell, augmented by about five water molecules of an extended first shell. The acid dissociation of HCl is visible from the proton transfer events observed in the QMCF MD simulation. The QMCF MD simulation shows several ligand exchange processes in the first hydration shell, which occur more frequently at the Cl site of the molecule.

Acknowledgments

Financial support for this work by the Thailand Research Fund (TRF) and Thailand Commission on Higher Education (ASEA-UNINET fellowships for C.K. and V.V.) are gratefully acknowledged and B.M.R. acknowledges support by the Austrian Science Foundation (FWF).

References

1. Kirk, K. L. Biochemistry of Halogens and Inorganic Halides; Plenum Press: New York, 1991.
2. Amirand, C.; Maillard, D. J Mol Struct 1988, 176, 181.
3. Triolo, R.; Narten, A. H. J Chem Phys 1975, 63, 3624.
4. Agmon, N. J Phys Chem A 1998, 102, 192.
5. Fárník, M.; Weimann, M.; Suhm, M. A. J Chem Phys 2003, 118, 10120.
6. Cappa, C. D.; Smith, J. D.; Messer, B.; Cohen, R. C.; Saykally, R. J. J Phys Chem B 2006, 110, 1166.
7. Botti, A.; Bruni, F.; Ricci, M. A.; Soper, A. K. J Chem Phys 2006, 125, 14508.
8. Chipot, C.; Gorb, L. G.; Rivail, J. L. J Phys Chem 1994, 98, 1601.
9. Robertson, S. H.; Clary, D. C. Faraday Discuss 1995, 100, 309.
10. Gertner, B. J.; Hynes, J. T. Science 1996, 271, 1563.
11. Planas, M.; Lee, C.; Novoa, J. J. J Phys Chem 1996, 100, 16495.
12. Laasonen, K.; Klein, M. L. J Am Chem Soc 1994, 116, 11620.
13. Packer, M. J.; Clary, D. C. J Phys Chem 1995, 99, 14323.
14. Balbuena, P. B.; Johnston, K. P.; Rossky, P. J. J Phys Chem 1996, 100, 2716.
15. Lee, C.; Sosa, C.; Planas, M.; Novoa, J. J Chem Phys 1996, 104, 7081.
16. Laasonen, K.; Klein, M. L. J Phys Chem A 1997, 101, 98.
17. Ando, K.; Hynes, J. T. J Phys Chem B 1997, 101, 10464.
18. Geiger, F. M.; Hicks, J. M.; de Dios, A. C. J Phys Chem A 1998, 102, 1514.
19. Re, S.; Osamura, Y.; Suzuki, Y. J Chem Phys 1998, 109, 973.

20. Bacelo, D. E.; Binning, R. C.; Ishikawa, Y. J Phys Chem A 1999, 103, 4631.
21. Chaban, G. M.; Gerber, R. B.; Janda, K. C. J Phys Chem A 2001, 105, 8323.
22. Cabaleiro-lago, E. M.; Hermida-Ramón, J. M.; Rodríguez-Otero, J. J Chem Phys 2002, 117, 3160.
23. Masia, M.; Forbert, H.; Marx, D. J Phys Chem A 2007, 111, 12181.
24. Buch, V.; Dubrovskiy, A.; Mohamed, F.; Parrinello, M.; Sadlej, J.; Hammerich, A. D.; Devlin, J. P. J Phys Chem A 2008, 112, 2144.
25. Lee, H.-S.; Tuckerman, M. E. J Phys Chem A 2009, 113, 2144.
26. Heuft, J. M.; Meijer, E. J. Phys Chem Chem Phys 2006, 8, 3116.
27. Rode, B. M.; Schwenk, C. F.; Tongraar, A. J Mol Liq 2003, 110, 105.
28. Rode, B. M.; Schwenk, C. F.; Hofer, T. S.; Randolf, B. R. Coord Chem Rev 2005, 249, 2993.
29. Rode, B. M.; Hofer, T. S.; Randolf, B. R.; Schwenk, C. F.; Xenides, D.; Vchirawongkwin, V. Theor Chem Acc 2006, 115, 77.
30. Field, M. J.; Bash, P. A.; Karplus, M. J Comput Chem 1990, 11, 700.
31. Gao, J. J Am Chem Soc 1993, 115, 2930.
32. Bakowies, D.; Thiel, W. J Phys Chem 1996, 100, 10580.
33. Stillinger, F. H.; Rahman, A. J Chem Phys 1978, 68, 666.
34. Bopp, P.; Janscó, G.; Heinzinger, K. Chem Phys Lett 1983, 98, 129.
35. Brooks, B. R.; Bruccoleri, R. E.; Olafson, B. D.; States, D. J.; Swaminathan, S.; Karplus, M. J Comput Chem 1983, 4, 187.
36. Kritayakornupong, C.; Vchirawongkwin, V.; Hofer, T. S.; Rode, B. M. J Phys Chem B 2008, 112, 12032.
37. Vchirawongkwin, V.; Rode, B. M.; Persson, I. J Phys Chem B 2007, 111, 4150.
38. Fatmi, M. Q.; Hofer, T. S.; Randolf, B. R.; Rode, B. M. J Comput Chem 2007, 28, 1704.
39. Hofer, T. S.; Randolf, B. R.; Shah, S. A. A.; Rode, B. M.; Persson, I. Chem Phys Lett 2007, 445, 193.
40. Berendsen, H. J. C.; Postma, J. P. M.; van Gunsteren, W. F.; DiNola, A.; Haak, J. R. J Chem Phys 1984, 81, 3684.
41. Adams, D. J.; Adams, E. H.; Hills, G. J Mol Phys 1979, 38, 387.
42. Ahlrichs, R.; Bär, M.; Häser, M.; Horn, H.; Kölmel, C. Chem Phys Lett 1989, 162, 165.
43. Ahlrichs, R.; von Arnim, M. Methods and Techniques in Computational Chemistry: METECC-95; Cagliari: Sardinia, 1995.
44. von Arnim, M.; Ahlrichs, R. J Comput Chem 1998, 19, 1746.
45. Dunning, T. H., Jr.; Wadt, W. R. J Chem Phys 1989, 90, 1007.
46. Dunning, T. H., Jr.; Hay, P. J. Modern Theoretical Chemistry: Methods of Electronic Structure Theory, Vol. 3; Schaefer, H. F., III, Ed.; Plenum Press: New York, 1977.
47. D'Incal, A.; Hofer, T. S.; Randolf, B. R.; Rode, B. M. Phys Chem Chem Phys 2006, 8, 2841.
48. Hofer, T. S.; Pribil, A. B.; Randolf, B. R.; Rode, B. M. J Am Chem Soc 2005, 127, 14231.
49. Hofer, T. S.; Randolf, B. R.; Rode, B. M. Phys Chem Chem Phys 2005, 7, 1382.
50. Hofer, T. S.; Rode, B. M.; Randolf, B. R. Chem Phys 2005, 312, 81.
51. Schwenk, C. F.; Hofer, T. S.; Rode, B. M. J Phys Chem A 2004, 108, 1509.
52. Schwenk, C. F.; Löfffler, H. H.; Rode, B. M. J Chem Phys 2001, 115, 10808.
53. Xenides, D.; Randolf, B. R.; Rode, B. M. J Chem Phys 2005, 122, 174506.
54. Herzberg, G.; Spink, J. W. T. Z Phys 1934, 89, 474.
55. Huber, K. P.; Herzberg, G.Molecular Spectra and Molecular Structure, Vol. 37; Van Nostrand Reinhold: New York, 1979.
56. Franks, F. Water: A Comprehensive Treatise, Vol. 1; Plenum Press: New York, 1972.
57. Shimanouchi, T. Tables of Molecular Vibrational Frequencies, Vol. 37; National Bureau of Standards: Washington, D.C., 1972.
58. Chase, M. W.; Davies, C. A.; Downey, J. R.; Frurip, D. J.; McDonald, R. A.; Syverud, A. N. J Phys Chem Ref Data Suppl 1985, 14.
59. Yoo, S.; Zeng, X. C.; Xantheas, S. S. J Chem Phys 2009, 130, 221102.
60. Hofer, T. S.; Tran, H. T.; Schwenk, C. F.; Rode, B. M. J Comput Chem 2004, 25, 211.
61. Lock, A. J.; Woutersen, S.; Bakker, H. J. J Phys Chem A 2001, 105, 1238.

Structural and Dynamical Properties and Vibrational Spectra of Bisulfate Ion in Water: A Study by *Ab Initio* Quantum Mechanical Charge Field Molecular Dynamics

Viwat Vchirawongkwin,*,† Chinapong Kritayakornupong,‡ and Bernd M. Rode§

Department of Chemistry, Faculty of Science, Chulalongkorn University, Phayathai Road, Patumwan, Bangkok 10330, Thailand, Department of Chemistry, Faculty of Science, King Mongkut's University of Technology Thonburi, Bangkok 10140, Thailand, and Theoretical Chemistry Division, Institute of General, Inorganic and Theoretical Chemistry, University of Innsbruck, Innrain 52a, A-6020 Innsbruck, Austria

Received: June 6, 2010; Revised Manuscript Received: August 2, 2010

The *ab initio* quantum mechanical charge field molecular dynamics (QMCF MD) formalism was applied to simulate the bisulfate ion, HSO_4^-, in aqueous solution. The averaged geometry of bisulfate ion supports the separation of six normal modes of the O*−SO_3 unit with C_{3v} symmetry from three modes of the OH group in the evaluation of vibrational spectra obtained from the velocity autocorrelation functions (VACFs) with subsequent normal coordinate analyses. The calculated frequencies are in good agreement with the observations in Raman and IR experiments. The difference of the averaged coordination number obtained for the whole molecule (8.0) and the summation over coordinating sites (10.9) indicates some water molecules to be located in the overlapping volumes of individual hydration spheres. The averaged number of hydrogen bonds (H-bonds) during the simulation period (5.8) indicates that some water molecules are situated in the molecular hydration shell with an unsuitable orientation to form a hydrogen bond with the ion. The mean residence time in the surroundings of the bisulfate ion classify it generally as a weak structure-making ion, but the analysis of the individual sites reveals a more complex behavior of them, in particular a strong interaction with a water molecule at the hydrogen site.

Introduction

Bisulfate ion is produced by the first deprotonation of sulfuric acid, playing an important role to form hygroscopic aerosols in the atmosphere.[1−4] The vibrational spectra of bisulfate ion were investigated by *in situ* Fourier transform infrared (FTIR) spectroscopy of molecular adsorption on the surface of Pt single crystal electrodes,[5] producing anomalous peaks from the adsorption and desorption of submonolayers of strongly bound hydrogen.[6,7] The fundamental vibrational frequencies of HSO_4^- ion were also assigned within the infrared spectra of concentrated solution in the spectral region of 600−1500 cm^{-1}.[8] The Raman studies of aqueous NH_4HSO_4 solutions over a broad concentration and temperature range indicate that the bisulfate ion is the dominant species above 250 °C and possesses C_{3v} symmetry in dilute solutions.[9,10] The phase diagram for the NH_4HSO_4/H_2O system presented a low-temperature crystalline phase composed of NH_4HSO_4 with eight water molecules.[11] Although the properties of bisulfate ion have been investigated in many experiments, most theoretical treatments were only interested in the system of hydrated sulfuric acid.[12−17] This motivated our interest to investigate the vibrational spectra and the structural and dynamical properties for the HSO_4^- ion and its hydration shell in aqueous solution.

The specific investigation of an aqueous bisulfate system is difficult by experiment, due to a mixture of sulfate and hydronium ions produced by the second dissociation of sulfuric acid. Computer simulations have become an alternative tool to gain access to solvate microspecies properties needed for the interpretation of experimental observations and the chemical behavior. The structural and dynamical properties of hydrated bisulfate ion are of great significance for the detailed understanding of all chemical processes of this ion in aqueous solution. However, the bisulfate ion is a composite structure difficult to access by a conventional QM/MM method, because of the complicated and asymmetric potential energy hypersurface describing the interaction between the HSO_4^- ion and water. An *ab initio* quantum mechanical charge field molecular dynamics (QMCF MD) formalism,[18,19] however, does not require an analytical solute−solvent potential, and hence, this method has already been successfully employed to investigate the structural and dynamical properties of the hydrated sulfate,[20,21] phosphate,[22,23] perchlorate,[22,24] and bicarbonate[25,26] anions. In this work, the QMCF MD method was used to simulate the hydrated HSO_4^- ion in order to obtain its structure and some dynamical properties, and also the vibrational spectra of all normal modes evaluated by means of the velocity autocorrelation functions (VACFs). The structural properties for each hydration site and the overall molecular shell were obtained via radial distribution functions (RDFs), coordination number distributions (CNDs), and angular distribution functions (ADFs). The dynamics were characterized by means of ligand mean residence times (MRTs). We also evaluated structural and dynamical properties by means of the molecular approach equivalent to the "solvent-accessible surface" referred to in previous work.[25]

Methods

The *ab initio* quantum mechanical charge field molecular dynamics (QMCF MD) formalism has been outlined in detail elsewhere.[18,19] Due to the inclusion of an additional quantum mechanically treated solvent *layer zone* located beyond the first hydration shell of the solute species, the QMCF method does

* To whom correspondence should be addressed. E-mail: Viwat.V@Chula.ac.th.
† Chulalongkorn University.
‡ King Mongkut's University of Technology Thonburi.
§ University of Innsbruck.

10.1021/jp105181n
Published on Web 08/13/2010

not require the construction of potential functions between the solute and water molecules; i.e., it avoids a time-consuming and sometimes hardly manageable task necessary in the conventional quantum mechanical/molecular mechanical molecular dynamics (QM/MM MD) formalism.[27−30] A further advantage of the QMCF MD method is the inclusion of the point charges of the atoms in the MM region with their changing positions in the core Hamiltonian for the QM region via a perturbation term

$$V' = \sum_{i=1}^{n} \sum_{j=1}^{m} \frac{q_j^{\mathrm{MM}}}{r_{ij}} \tag{1}$$

where n is the number of atoms in the QM region, m is the number of atoms in the MM region, q_j^{MM} is the partial charges of these atoms according to the selected water model, and r_{ij} refers to the distance between a pair of particles in the QM (i) and MM (j) regions. On the other hand, the dynamically changing charges of QM particles, q_i^{QM}, determined by population analysis contribute to the force on each atom j in the MM region as Coulombic forces

$$F_j^{\mathrm{QM}\rightarrow\mathrm{MM}} = \sum_{i=1}^{n} \frac{q_i^{\mathrm{QM}} \cdot q_j^{\mathrm{MM}}}{r_{ij}} \tag{2}$$

As the conventional QM/MM MD formalism, the QMCF MD method allows the migration of water molecules between the QM and MM region. For this process, one has to apply a smoothing function[31]

$$S(r) = \begin{cases} 0 & \text{for } r > r_{\mathrm{on}} \\ \dfrac{(r_{\mathrm{off}}^{\,2} - r^2)^2(r_{\mathrm{off}}^{\,2} + 2r^2 - 3r_{\mathrm{on}}^{\,2})}{(r_{\mathrm{off}}^{\,2} - r_{\mathrm{on}}^{\,2})^3} & \text{for } r_{\mathrm{on}} \le r \le r_{\mathrm{off}} \\ 1 & \text{for } r < r_{\mathrm{off}} \end{cases} \tag{3}$$

where r is the distance of a given solvent molecule from the center of the simulation box, r_{off} is the radius of the QM region, and r_{on} is the inner border of the smoothing region. The formalism is applied to all atoms of molecules located in the smoothing region, ensuring a continuous transition and change of forces for these molecules according to

$$F_j^{\mathrm{smooth}} = F_j^{\mathrm{MM}} + (F_j^{\mathrm{layer}} - F_j^{\mathrm{MM}}) \times S(r) \tag{4}$$

where F_j^{layer} is the force acting on a particle j located in the (outer QM) smoothing zone and F_j^{MM} is the force acting on a particle j in the MM region. In this context, it has to be mentioned that energy is not rigorously conserved, but the related error can be considered very minor due to the short simulation time and the large size of the quantum mechanical region.

The bisulfate solution consisted of one bisulfate ion and 496 water molecules in a cubic box of 24.67 Å with the periodic boundary condition. The density of the simulation box was 0.997 g cm^{-3}, i.e., the experimental value of pure water at 298 K. The simulation was performed in the *NVT* ensemble using a general predictor-corrector algorithm with a time step of 0.2 fs. The system temperature was maintained at 298.16 K by the Berendsen temperature-scaling algorithm[32] with a relaxation time of 100 fs. The QM subregions, namely, the core and layer zone, extended to 3.5 and 6.0 Å, respectively. The quantum mechanical calculation was performed by means of the Hartree−Fock (HF) method with the Dunning double-ζ plus polarization (DZP)[33,34] basis sets for hydrogen, sulfur, and oxygen atoms in the QM region, i.e., the same theoretical level employed in our previous study of the hydrated sulfate ion.[20] The thickness of the smoothing region was chosen as 0.2 Å with the values of r_{on} and r_{off} as 5.8 and 6.0 Å, respectively, according to the radial distribution function (RDF) obtained from the equilibrated simulation. The selected water model applied to calculate the interactions between pairs of water in the MM region was the flexible BJH−CF2 model,[35,36] with cutoff distances of 3.0 and 5.0 Å for non-Coulombic interactions between H atoms and between O and H atoms, respectively. The partial charges for oxygen and hydrogen atoms in the water molecule according to the BJH−CF2 model are −0.65966 and +0.32983. This water model supports the fully flexible molecular geometries of water molecules transiting between the QM and MM region. The Coulombic interactions between the Mulliken charges on the atoms within the QM region and the point charges of water molecules according to the BJH−CF2 model are evaluated providing an electrostatic description by a dynamically charging field of point charges, which change according to the movements of atoms inside the QM region and water molecules in the MM region in the course of the simulation. This ensures the continuous adaptation of the Coulombic interactions to all polarization and charge-transfer effects within solute and surrounding solvent layers.[18,19] In addition, the reaction field method combined with the shifted-force potential technique were applied to account for long-range electrostatic potentials and forces, with a spherical cutoff limit of 12.350 Å. The system was equilibrated with the QMCF MD method for 50 000 steps (10 ps), and a further 50 000 steps (10 ps) were collected as data sampling for analyzing the structural and dynamical properties. On average, 24.8 water molecules were present in the QM region.

The structural and dynamical properties for the hydration shell of HSO_4^- ion were not only evaluated for individual atoms but also in a molecular manner. The molecular hydration shell of bisulfate ion was constructed by the combination of all atomic hydration spheres of the ion. The coordinating site for each water molecule to the bisulfate ion was defined by searching for the shortest distance between the oxygen atom of the water molecule and each atom within the ion.[25] The molecular radial distribution functions (RDFs), molecular coordination number distributions (CNDs), and molecular ligand mean residence times (MRTs) for the hydration shell of bisulfate ion are thus presented in this Article. All MRT values were evaluated by the direct method,[37] counting the water exchange processes between hydration shell and bulk. The most appropriate time span to record a water displacement from its original coordination sphere as an exchange process is 0.5 ps,[37,38] which corresponds to the average lifetime of a hydrogen bond in the solvent.[39]

The dynamical properties of a fluid system related to macroscopic transport coefficients can be evaluated from the velocity autocorrelation functions (VACFs), and their Fourier transformations can be interpreted as the vibrational spectra. The vibrational spectra of bisulfate ion were obtained from the VACFs using normal-coordinate analysis.[40] The normalized VACF, $C(t)$, is defined as

$$C(t) = \frac{\sum_{i}^{N_t}\sum_{j}^{N} v_j(t_i)v_j(t_i + t)}{N_t N \sum_{i}^{N_t}\sum_{j}^{N} v_j(t_i)v_j(t_i)} \quad (5)$$

where N is the number of particles, N_t is the number of time origins t_i, and v_j denotes a certain velocity component of the particle j. A correlation length of 2.0 ps was used to obtain the power spectra with 4000 averaged time origins.

Results and Discussion

Structural and Dynamical Properties of HSO_4^- Ion. Due to the dynamic motion of all atoms within the system during the simulation period, all structural parameters such as bonds, angles, and dihedral angles within the bisulfate ion required to construct the geometry of the ion were collected with their statistical deviation listed in Table 1. The averaged geometry of HSO_4^- ion constructed from the structural parameters in Table 1 is shown in Figure 1. The average S═O distances vary within 0.070 Å and are slightly shorter than those in the SO_4^{2-} ion[20] by 0.02 Å, while the single bond of S to O(4) is significantly longer with 1.585 Å. The average O—H distance of 0.975 Å for the HSO_4^- ion is slightly longer than the distance of the analogous bond in the HCO_3^- ion[25] by ∼0.02 Å. The bond and dihedral angles were collected in the form of angular distribution functions (ADFs). The average bond angles around the sulfur atom again indicate the similarity of terminal oxygens and the unique property of O(4). In contrast to the strong flexibility of the ∠CO(3)H angle of the HCO_3^- ion,[25] the ∠SO(4)H ADF shows a deviation of only 9°. Our selected theoretical level, HF/DZP, for the QMCF MD simulation was validated by comparing the structural parameters with those obtained from various methods evaluated in the gas phase and solution using the polarizable continuum model (PCM).[42] The hybrid B3LYP exchange-correlation functional coupling with the tzvp+ basis set[43] was employed to verify the interpretation of the spectra of photoelectron spectroscopy for the HSO_4^- ion;[41] thus, we also utilized this basis set coupling with the Hartree—Fock (HF), B3LYP, and quadratic CI calculation including single and double substitutions (QCISD) levels to optimized the geometry of HSO_4^- in both phases. The HF/DZP level was also performed to investigate the effect of isotropic and uniform field generated by the PCM to the geometry of HSO_4^- ion. All optimized geometries in gas and solution phase were found to have C_s symmetry. The effect of PCM on the geometry of HSO_4^- ion presents slightly longer bonds of terminated oxygen and O(4)—H bond, and a slightly shorter S—O(4) bond. The structural parameters obtained from the QMCF MD simulation show a similar changing pattern to the PCM model but presenting a slightly stronger effect of explicit water molecules on the HSO_4^- ion compared with the HF/DZP results. Due to the fact that the structural parameters from the QCISD/tzvp+ optimization are within the deviation of those obtained from the QMCF MD simulation, this presents a suitability of the HF/DZP level to investigate the structural and dynamical properties of hydrated HSO_4^- ion.

The dihedral angle measured between the plane defined by the O(4)—S—O(1) and the hydrogen atom is one of the interesting structural characteristics, with a large deviation as shown in Table 1. The distribution of this angle within the simulation period is presented in Figure 2, showing a broad band with a main peak situated at 60° and an average dihedral angle of 40°. This angle distribution represents the ease of rotation for the hydrogen atom around the S—O(4) bond. This result agrees with the experimental result of a free rotation of OH group, treating the bisulfate ion with the C_{3v} symmetry.[9,10] We also utilized this approximation to separate three modes of the OH group, namely, O—H stretching (ν(OH)), S—O—H bending (δ(OH)), and S—O—H torsional (γ(OH)), from nine normal modes of the O*—SO_3 unit. The nine normal modes of the O*—SO_3 unit in C_{3v} symmetry will span the following representation:

$$\Gamma(C_{3v}) = 3a_1(\mathrm{R, ir}) + 3e(\mathrm{R, ir}) \quad (6)$$

In the Raman and infrared spectra under C_{3v} symmetry, the spectra will be predicted as only six bands, three of them becoming doubly degenerate modes. The power spectra of these normal modes for the HSO_4^- ion predicted by the QMCF MD simulation are displayed in Figure 3, and the frequencies of peaks for each mode are listed in Table 2. The ν_1 and ν_3 modes seemed to identify the characteristic of the O*—SO_3 unit in the HSO_4^- ion when it was investigated by Raman and IR experiments.[8−10] The calculated frequencies of these modes are in good agreement with the experimental data, again showing the reliability of QMCF MD simulation analyzing via VACFs the vibration modes of the solute.[21,26,44,45] It is interesting that the peak at 593 cm^{-1} [8] was only assigned as a characteristic frequency of HSO_4^- ion by Miller et al.[46] The peak of our calculation for the δ_6 mode located at 603 cm^{-1} corresponds to the observed data,[8,46] and hence, we assigned this mode to the characteristic frequency of HSO_4^- ion found in the cesium bromide region.[46] We also classified the frequency at 1341 cm^{-1} reported by Walrafen et al. as δ_4, as the other two totally symmetric (a_1) modes at 1050 and 885 cm^{-1} were identified as the ν_1 and ν_3 modes, respectively.[8] However, the peak of the δ_4 mode calculated by our VACF method at 635 cm^{-1} agrees with the assignment by Dawson et al. for this mode at 585 cm^{-1}.[10]

Our calculated spectra for the OH group present very broad bands, as shown in Figure 3B. The power spectrum of the ν(OH) mode also presents the frequency band coinciding with the the δ(OH) mode, due to the different orientation of the O—H bond for each time origin included in the evaluation of the ν(OH) mode producing the mixed modes. By our vector projection, the frequency bands of the ν(OH), δ(OH), and γ(OH) modes are found in the region of 2573—4039, 1075—1645, and 179—928 cm^{-1}, respectively. The ν(OH) mode shows the highest peak as a strong band at 3795 cm^{-1} and a weak band in the region 2573—3339 cm^{-1} in agreement with the assignment by the experiments.[8,10] The δ(OH) mode again is identified as characteristic of the OH group by the Raman and IR investigations,[8−10] and our calculated band with the peak at 1384 cm^{-1} for this mode is in good agreement with that. The projection of H's velocities onto a unit vector perpendicular to the S—O(4)—H plane for the γ(OH) mode presents two bands with peaks at 179 and 733 cm^{-1} for a weak and a strong band, respectively; this corresponds well with the assignment by Walrafen et al.[8]

The self-diffusion coefficient (D) of bisulfate ion was calculated from the center-of-mass VACF using the Green—Kubo relation[47]

$$D = \frac{1}{3}\lim_{t\to\infty}\int_0^t C(t)\,\mathrm{d}t \quad (7)$$

TABLE 1: Structural Parameters for the Geometry of HSO_4^- Ion Obtained from the Averaging of Their Distributions with Their Variations

		HF/DZP		HF/tzvp+		B3LYP/tzvp+		QCISD/tzvp+	
structural parameter	QMCF MD	gas	PCM	gas	PCM	gas[41]	PCM	gas	PCM
S−O(1) (Å)	1.453 ± 0.062	1.441	1.444	1.446	1.449	1.483	1.485	1.477	1.479
S−O(2) (Å)	1.455 ± 0.064	1.432	1.440	1.436	1.445	1.473	1.480	1.467	1.475
S−O(3) (Å)	1.454 ± 0.067	1.441	1.444	1.446	1.449	1.483	1.485	1.477	1.479
S−O(4) (Å)	1.585 ± 0.076	1.619	1.579	1.626	1.585	1.709	1.655	1.682	1.635
O(4)−H (Å)	0.975 ± 0.064	0.946	0.969	0.947	0.970	0.968	0.993	0.969	0.993
∠O(1)SO(2) (deg)	113 ± 7	115	114	115	114	116	114	116	114
∠O(1)SO(3) (deg)	113 ± 7	113	113	113	113	114	113	114	113
∠O(1)SO(4) (deg)	106 ± 7	104	106	104	106	104	106	104	106
∠SO(4)H (deg)	113 ± 9	108	112	107	110	104	108	104	108
O(3)SO(1)O(2) dihedral (deg)	−131 ± 7	−136	−132	−136	−132	−137	−133	−137	−133
O(4)SO(1)O(2) dihedral (deg)	114 ± 8	112	112	112	112	110	111	110	111
HO(4)SO(1) dihedral (deg)	40 ± 49	59	60	59	60	60	60	59	60

The calculated D value obtained from the QMCF MD simulation is 1.584×10^{-5} cm^2 s^{-1}, which is in good agreement with the experimental value of 1.385×10^{-5} cm^2 s^{-1}.[48] This again presents the success of the QMCF MD formalism to acquire the dynamical properties of hydrated composite solute.

Structural and Dynamical Properties of the Hydration Shell. With the QM radius of 6.0 Å, the average number of solvent molecules inside this region was 24.8 ± 6.3, during the simulation period. The coordinating sites of bisulfate ion consist of five atoms, namely, O(1) to O(4) and H, interacting with water molecules, and thus producing the hydration shell around this molecular solute. The structural property for each site was first evaluated by means of the radial distribution functions (RDFs) shown in Figure 4. The maximum and minimum distances of the hydration shell for each coordinating site obtained from the (site)−O_{water} and (site)−H_{water} are listed in Table 3. The shorter distances of a maximum and minimum for each O_s−H_{water} RDF compared to each related O_s−O_{water} RDF correspond to the orientation of water molecules pointing with hydrogen to the coordinating oxygens. Although the geometry analysis in the previous section has shown that the S−O bonds for the terminal oxygens O(1) to O(3) are almost identical, the hydration shells for each site present a different structure reflected by some variations of maximal and minimal distances in their RDFs. The RDFs of the hydration shell of O(2) represent a slightly more compact structure than those of the other two sites. With respect to the averaged geometry of HSO_4^- ion (see Figure 1), the O(2) site is far from the hydrogen atom so that the water molecules can hydrate this site with less perturbation from the hydrogen atom. The RDFs of O(4) atom show a more flexible hydration shell than the terminal oxygens,

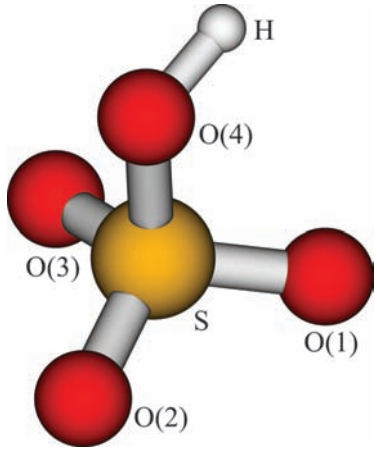

Figure 1. The averaged geometry of HSO_4^- ion constructed from the structural parameters of QMCF MD simulation presenting with the labels.

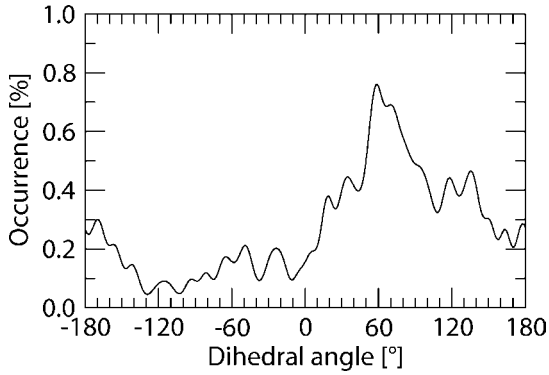

Figure 2. The distribution of H−O(4)−S−O(1) dihedral angle.

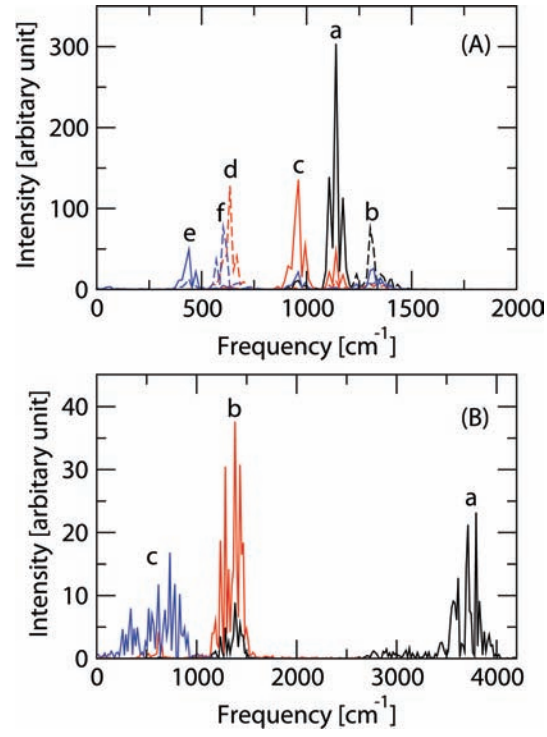

Figure 3. Power spectra of (A) the O*−SO_3 unit consisting of (a) ν_1, (b) ν_2, (c) ν_3, (d) δ_4, (e) δ_5, and (f) δ_6 modes and (B) three modes for the OH group consisting of (a) ν (OH), (b) δ (OH), and (c) γ (OH) modes.

TABLE 2: Vibration Frequencies (cm^{-1}) of Highest Peak for Each Normal Mode of HSO_4^- Ion Evaluated by the VACFs of QMCF MD Simulation, Given as Values Scaled by the Factor 0.902[21] in Parentheses

vibration mode	QMCF MD	Raman and IR
ν_1 symmetric SO_3 stretch, a_1	1140 (1028)	1050,[a] 1052,[b] 1050[c]
ν_2 asymmetric SO_3 stretch, e	1303 (1175)	1191,[a] 1230[c]
ν_3 S −(OH) stretch, a_1	961 (867)	899,[a] 898,[b] 885[c]
δ_4 symmetric SO_3 deformation, a_1	635 (573)	585,[a] 1341[c]
δ_5 asymmetric SO_3 deformation, e	440 (397)	422,[a] 417[c]
δ_6 SO_2 bending, e	603 (544)	593[c]
ν (OH)	3795 (3423)	2900,[a] 3000[c]
δ (OH)	1384 (1248)	1340,[a] 1240,[b] 1175−1250,[c] 1800[c]
γ(OH)	733 (661)	675−740[c]

[a] Raman data of 3.8 mol kg^{-1} NH_4HSO_4 solution at 25 °C.[10] [b] Raman data of 0.876 mol kg^{-1} NH_4HSO_4 solution at 22 °C.[9] [c] IR data of concentrated aqueous solutions of sulfuric acid in the region 290−4000 cm^{-1}.[8]

indicated by the flat shape and lower maximum of the O(4)−H_{water} RDF in the region assigned as hydration shell. The RDFs of H atom indicate the direction of the oxygen atom of water pointing to this site, and represent a well-defined structure by a strong peak in the H−O_{water} RDF.

The distances of the minima for each (site)−O_{water} RDF were employed to evaluate the coordination number distribution (CND) for the sites, as shown in Figure 5. Their averaged coordination numbers are also listed in Table 3 in the last column. The O(2) atom located in the far position from the hydrogen atom has the smallest coordination number among the oxygens and a significantly large average CND of O(3), again illustrating the different hydration structure for these oxygen atoms. The reasons for small deviations of the coordination numbers of the three terminated oxygen atoms are to be seen in slight deviations from the C_{3v} symmetry in the course of the simulation and the short sampling time, which would not cover sufficient orientations to include all possible configurations. Hence, the difference of 0.3 water molecules cannot be considered statistically significant. The actual effect of water molecules to each oxygen site requires further details as the average number of H-bonds, presented with the following analysis. The minimum of the O(4)−O_{water} RDF at 3.46 Å utilized to evaluate its CND also includes a part of the hydration shell of hydrogen atom. This leads to an overcounting of the coordination number for the composite molecular solute.[20,25] To clarify this problem, we again evaluated the RDF and CND for the molecular structure employing the distances of minimum for each (site)−O_{water} RDF as the criterion to assign the coordinating site for each water molecule shown in Figure 6. The characteristic values of molecular hydration shell and its averaged coordination number obtained from the molecular surface−water RDFs and CND are also listed in Table 3 in the last row.

The surface−O_{water} RDF presents two peaks at 1.80 and 2.90 Å in the region of 0.00−3.72 Å, corresponding to the hydration spheres of hydrogen and all oxygen atoms. The peak of O_s−O_{water} within the molecular RDF is well-defined and stronger than that in the individual O_s−O_{water} RDFs, representing more water molecules confined in the molecular hydration shell than those in the individual hydration spheres. However, the total average coordination number of 10.9 for all individual sites is larger than the average coordination number of 8.0 for the molecular hydration shell, showing an overcounting of ~3 water molecules, due to the overlap of individual hydration spheres as observed also in the hydration structures of sulfate[20] and bicarbonate[25] ions.

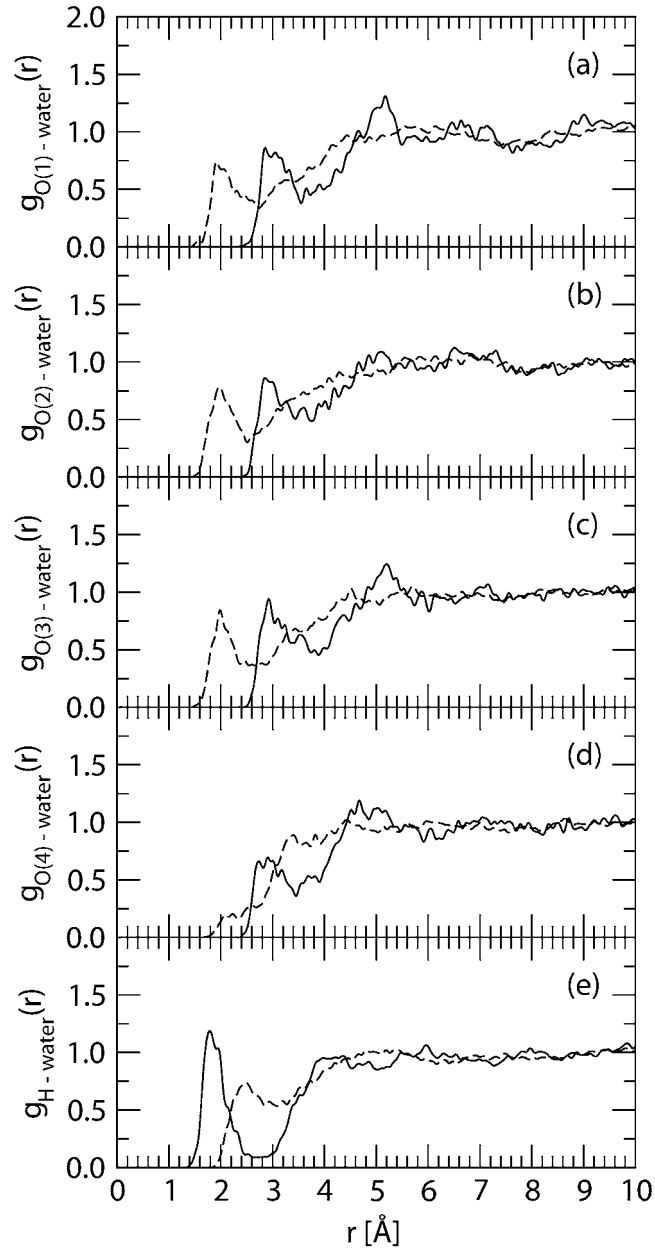

Figure 4. RDF plots of (a) O(1)−water, (b) O(2)−water, (c) O(3)−water, (d) O(4)−water, and (e) H−water; solid and dashed lines refer to the RDFs for the O and H atoms of water, respectively.

TABLE 3: Characteristic Values of the Radial Distribution Function $g_{\alpha\beta}(r)$ for Each Site of HSO_4^- Ion in the Hydration Shell Determined by the QMCF MD Simulation

coordinating site	$r_{max}(O_w)^a$	$r_{min}(O_w)^a$	$r_{max}(H_w)^a$	$r_{min}(H_w)^a$	n^a
O(1)	2.86	3.56	1.92	2.72	2.4
O(2)	2.86	3.44	1.98	2.52	2.1
O(3)	2.92	3.88	1.98	2.68	3.5
O(4)	2.90	3.46	2.22	3.34	1.9
H	1.78	2.64	2.48	3.08	1.0
surface	1.80, 2.90	2.42, 3.72	2.10	3.72	8.0

[a] r_{max} and r_{min} are the distances of the maximum and minimum of $g_{\alpha\beta}(r)$ for the hydration shell in Å, and n is the averaged coordination number of the shell, respectively.

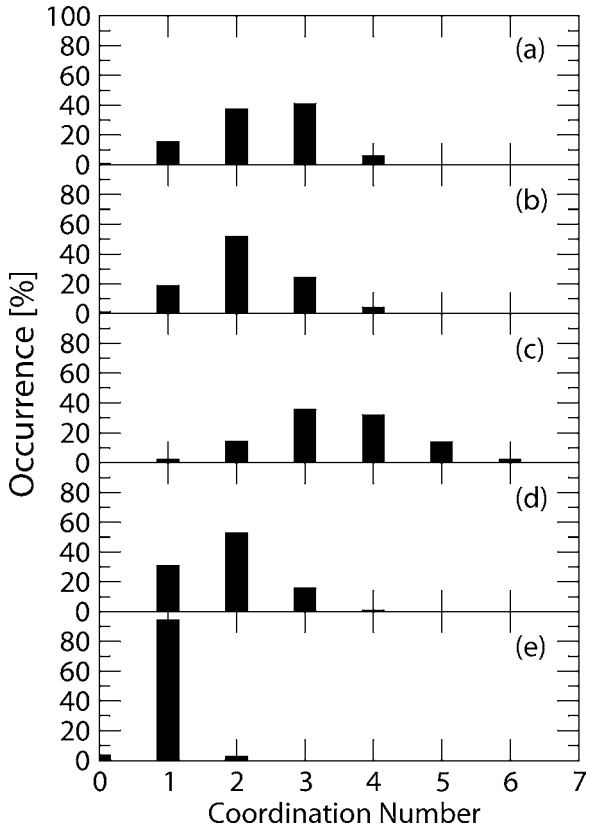

Figure 5. Hydration shell coordination number distributions of (a) O(1), (b) O(2), (c) O(3), (d) O(4), and (e) H atom of bisulfate ion.

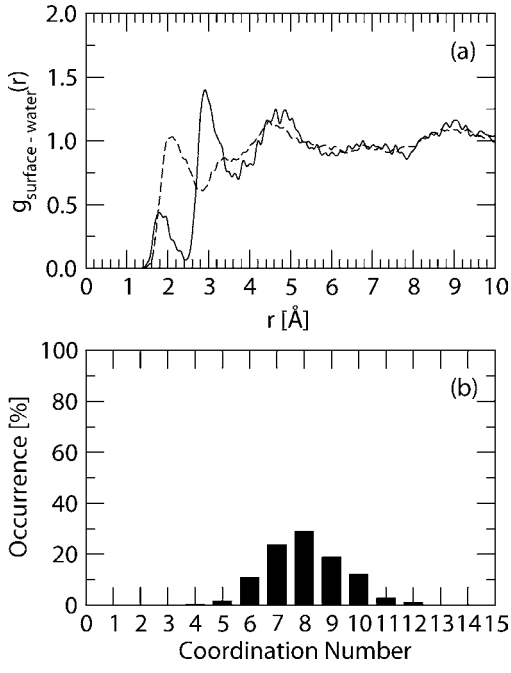

Figure 6. (a) Molecular RDF plots of HSO_4^- ion obtained from the QMCF MD simulation evaluated by means of the combination of spheres; solid and dashed lines refer to the RDFs for the O and H atoms of water, respectively. (b) The molecular hydration shell coordination number distribution of the HSO_4^- ion.

The orientation of water molecules in the individual hydration spheres was investigated by means of the angular distribution function (ADF) of $O_w-H_w\cdots$(site) angles, shown in Figure 7. These ADFs show a similar pattern with two peaks located at ca. 60 and 160°, corresponding to the two hydrogens of

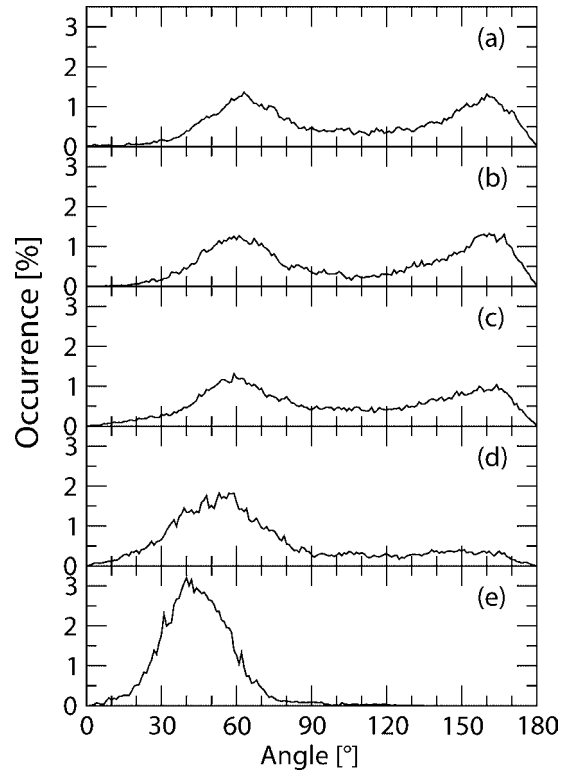

Figure 7. $O_w-H_w\cdots$(site) ADFs for (a) O(1), (b) O(2), (c) O(3), (d) O(4), and (e) H atom of HSO_4^- ion.

hydrating water molecules. The H_{water} atom pointing to the terminal oxygen sites is represented by the large angles. The ADF of O(4) displays a different orientation of hydrating water molecules with a high probability of small angles and very low probability of large angles, indicating that most of the H_{water} atoms do not point to this site.

According to the dynamical movements of all atoms within the system, the number of H-bonds between the bisulfate ion and the hydrating water molecules fluctuates during the simulation period. Since the definition of H-bond has been expressed in two different ways, namely, an energetic and a geometric criterion,[49,50] we utilized the structural criterion depending on the cutoff parameters (distances $R_{HO}^{(c)}$ and $R_{OO}^{(c)}$ and angle $\phi^{(c)}$) in analogy to water−dimethyl sulfoxide mixtures[51] and hydrated bicarbonate ion.[26] The cutoff distances $R_{HO}^{(c)}$ and $R_{OO}^{(c)}$ for each oxygen site were obtained from the corresponding (O_s-H_{water} and O_s-O_{water}) RDFs, while the cutoff parameters for the hydrogen site employed the distances of the first boundary in the $H-O_{water}$ and $O(4)-O_{water}$ RDFs, respectively. The angle $\phi^{(c)}$ was set to 30°.[51] The number of H-bonds as a function of time for each site is shown in Figure 8, presenting an average number of H-bonds of 1.5 ± 0.8, 1.5 ± 0.8, 1.6 ± 0.8, 0.4 ± 0.5, and 0.9 ± 0.3 for the O(1), O(2), O(3), O(4), and H sites, respectively. The smaller average number of H-bonds compared with the corresponding average coordination number for each hydration site indicates that some water molecules located in the hydration shell actually coordinate with the bisulfate ion, while others have an unsuitable orientation to form an H-bond. The slight difference of the average number of H-bonds for the O(1), O(2), and O(3) again presents the identical characteristics of these sites, corresponding to the C_{3v} symmetry. This difference for the O(4) site (ca. 1.5 molecules) clarifies the inclusion of extra water molecules from the hydration shell of the H site, and proves a weak interaction with water molecules at this site. The average number of H-bonds (5.8) compared

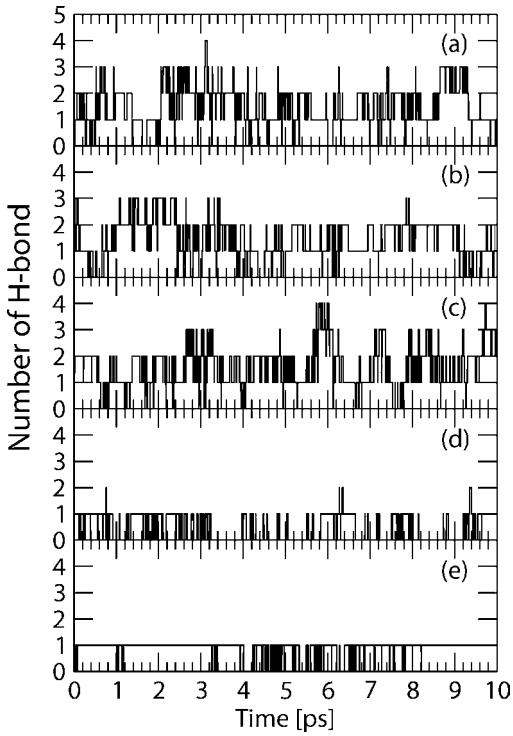

Figure 8. Number of hydrogen bonds between (a) O(1), (b) O(2), (c) O(3), (d) O(4), and (e) H atom of HSO_4^- ion and water molecules within the hydration shell during 10 ps of the QMCF MD simulation.

with the average coordination number (8.0) for the molecular ion shows that ~2 water molecules are located in the molecular hydration shell without forming H-bonds to the bisulfate ion, however.

The dynamical properties of water molecules hydrating the bisulfate ion were investigated by the ligand mean residence time (MRT) evaluated by the direct method,[37] from the average number of water molecules in the hydration shell during the simulation and from the number of exchange events for two time parameters $t^* = 0.0$, defined as the minimum duration of a ligand displacement from its original shell to account for an exchange process. t^* was set to 0.5 ps in accordance with the average lifetime of a hydrogen bond,[39] whereas $t^* = 0.0$ counts all exchange attempts. All MRT values for individual oxygen and hydrogen sites were summarized in Table 4. The total number of water molecules counted for individual exchange processes of all oxygens and hydrogen were 90 and 37, being larger than those counted for the molecular hydration shell (33 and 19). The total number of attempted and lasting exchange processes of individual atoms evaluated at $t^* = 0.0$ ps (576 events) and $t^* = 0.5$ ps (73 events), respectively, are also higher than the 410 and 39 events counted by the molecular approach, which avoids counting water molecules within the intersection of individual hydration spheres. The difference in exchange processes (73 and 39, respectively) shows that half of the exchange events are actually migrations of water molecules between the coordinating sites of HSO_4^- ion, similar to the HCO_3^- system.[25] The number of processes needed for one successful water exchange, R_{ex}, for the terminal oxygen atoms indicates a weak interaction with the water molecules in their vicinity compared to the hydrogen site. The peculiar value of R_{ex} for the O(4) site stems from the partial inclusion of the hydration sphere of the hydrogen site. The standard relaxation time used in the direct method with $t^* = 0.5$ ps leads to the MRT of water ligands at the coordination sites, while the

TABLE 4: Mean Ligand Residence Time τ in ps, Number of Accounted Ligand Exchange Events N, and Total Number of Processes Needed for One Successful Water Exchange R_{ex} Obtained from the QMCF Simulation

	$t^* = 0.0$ ps			$t^* = 0.5$ ps			
	N_{inv}^a	$N_{ex}^{0.0}$/10 ps^b	$\tau_D^{0.0\,c}$	N_{inv}^a	$N_{ex}^{0.5}$/10 ps^b	$\tau_D^{0.5\,c}$	R_{ex}^d
O(1)	17	118	0.20	10	19	1.27	6.2
O(2)	19	131	0.17	8	21	1.04	6.2
O(3)	25	160	0.22	12	24	1.47	6.7
O(4)	22	110	0.17	5	7	2.72	15.7
H	7	57	0.17	2	2	4.95	28.5
surface	33	410	0.19	19	39	2.02	10.5
H_2O^e		269[37]	0.2,[37] 0.33[38]		24[37]	1.7,[37] 1.51[38]	11.2[37]
H_2O^f		131[52]	0.2,[52] 0.55[39]		20[52]	1.3[52]	6.5[52]

[a] Number of ligands involved in the MRT evaluation according to the value of t^*. [b] Number of accounted exchange events per 10 ps lasting at least 0.0 and 0.5 ps, respectively. [c] Mean residence time determined by the direct method[37] in ps. [d] Average number of processes needed for one successful ligand exchange. [e] Values obtained from a QM/MM-MD simulation of pure water[37,38] in ps. [f] Values obtained from a QMCF MD simulation of pure water[52] in ps.

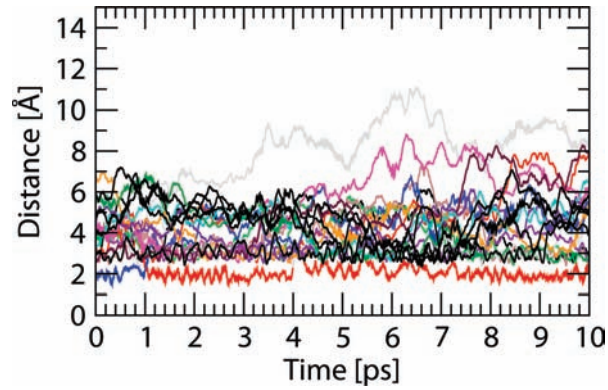

Figure 9. Distance plot of the molecular anion sites and oxygen atom of water as a function of time during the QMCF MD simulation period.

hydrogen bond lifetimes can be estimated with $t^* = 0.0$ ps.[25,37] The corresponding value obtained from the simulation of the pure water system based on the QM/MM MD formalism is 0.33 ps; the $t^* = 0.0$ values account for each hydrogen bond making/breaking process.[38] Both mean residence times and hydrogen bond lifetimes for the individual sites and the molecular ion as a whole prove HSO_4^- as a weak structure-making ion. This effect is not evenly distribution to all sites of the ion but most pronounced near the hydrogen site, as shown in Figure 9. This plot presents the distances of all water molecules within the molecular hydration shell measured from each coordinating site. After an exchange of water molecules binding to the hydrogen site at 1.0 ps, the water molecule retained the interaction with this site until the end of sampling time. Structure breaking/making is commonly regarded as a property related to the dynamics of the water molecules in the surrounding of a solute. If it was defined only as a structural effect, any kind of solute would break some H bonds of the solvent and hence its structure. However, in a dynamical sense, structure making means the formation of a layer of solvent molecules around the solute with lower mobility, while structure breaking would mean that the surrounding solvent molecules are more mobile than the solvent molecules in the bulk. Although the Berendsen temperature-scaling algorithm[32] requires in principle a long simulation period to sufficiently describe the phase space, a large number of

successful simulations published indicate that our simulation time of 10 ps is adequate to reproduce well the properties of hydrated ions, and thus also of the bisulfate ion. Comparing results for exchange dynamics and H-bond life times for simulations of pure water[38] and experimental results[39] the HF method seems to be a good compromise between accuracy and affordable computational effort to estimate dynamical effects as well. Although HF and the methodical problems associated with the thermostatisation probably lead to slightly underestimated values, the associated errors are probably within a 10 − 20% range.

As HSO_4^- ion is still a fairly strong acid in water, a dissociation process could be expected to be observable. However, this is a function not only of the thermodynamics but also of the kinetics, and even in the case of a much stronger acid, namely, HCl, despite a number of attempted proton transfers within 10 ps of simulation, no full proton transfer could be observed.[45] There is no doubt that, over a much longer simulation time, such a process would occur, however.

Conclusion

Our QMCF MD simulation results for hydrated bisulfate ion are well compatible with the Raman and IR experiments, assuming C_{3v} symmetry.[9,10] The vector projection of each vibration mode coupling with the VACF calculations gives the vibrational frequencies in good agreement with the experimental observations, especially of the characteristic modes.[8−10] These results again indicate the success and reliability of our approach to investigate the properties of composite hydrated anions.[20−26] The HSO_4^- ion is characterized as a weakly structure-making ion in aqueous solution, slightly weaker than the sulfate ion.[20] The hydrogen site forms a significant hydration structure characterized by a strong H-bond with one water. This stronger interaction of the hydrogen site of the HSO_4^- ion compared to that of the HCO_3^- ion reflected by the mean residence times of water ligands at the hydrogen site of 4.95 for the HSO_4^- and 0.82 for HCO_3^- [25] clearly demonstrates the higher acidity of HSO_4^-. The water molecules hydrating the bisulfate ion have a high mobility, reflected by rapidly changing binding sites and orientations while forming and breaking H-bonds with the ion. To describe these effects by classical or conventional QM/MM molecular dynamics would be a most difficult task, as it would have required the construction of analytical interaction potential functions taking into account all the asymmetry of the interaction between solute and solvent, which in the case of bisulfate would be difficult and subject to many possible error sources and inaccuracies.

Acknowledgment. Generous financial support by the Austrian Science Foundation (FWF) and ASEA-UNINET, the Thailand Research Fund and Thailand Commission on Higher Education (fellowships for V.V. and C.K.), Faculty of Science, Chulalongkorn University (RES A1 B1-19 for V.V.), and Center for Petroleum, Petrochemicals and Advanced Materials, Chulalongkorn University are gratefully acknowledged.

References and Notes

(1) Calhoun, J. A.; Charlson, R. J.; Bates, T. S. *Geophys. Res. Lett.* **1991**, *18*, 1877–1880.

(2) Charlson, R. J.; Schwartz, S. E.; Hales, J. M.; Cess, R. D.; Coakley, J. A., Jr.; Hansen, J. E.; Hofmann, D. J. *Science* **1992**, *255*, 423–430.

(3) Laaksonen, A.; Talanquer, V.; Oxtoby, D. W. *Annu. Rev. Phys. Chem.* **1995**, *46*, 489–524.

(4) Bianco, R.; Hynes, J. T. *Acc. Chem. Res.* **2006**, *39*, 159–165.

(5) Faguy, P. W.; Marinković, N. S.; Adžić, R. R. *Langmuir* **1996**, *12*, 243–247.

(6) Clavilier, J. *J. Electroanal. Chem.* **1980**, *107*, 211–216.

(7) Faguy, P. W.; Marinkovic, N.; Adzic, R. R.; Fierro, C. A.; Yeager, E. B. *J. Electroanal. Chem.* **1990**, *298*, 245–262.

(8) Walrafen, G. E.; Dodd, D. M. *Trans. Faraday Soc.* **1961**, *57*, 1286–1296.

(9) Rudolph, W. *Z. Phys. Chem.* **1996**, *194*, 73–95.

(10) Dawson, B. S. W.; Irish, D. E.; Toogood, G. E. *J. Phys. Chem.* **1986**, *90*, 334–341.

(11) Imre, D. G.; Xu, H.; Tang, I. N.; McGraw, R. *J. Phys. Chem. A* **1997**, *101*, 4191–4195.

(12) Re, S.; Osamura, Y.; Morokuma, K. *J. Phys. Chem. A* **1999**, *103*, 3535–3547.

(13) Ding, C.-G.; Laasonen, K. *Chem. Phys. Lett.* **2004**, *390*, 307–313.

(14) Choe, Y.-K.; Tsuchida, E.; Ikeshoji, T. *J. Chem. Phys.* **2007**, *126*, 154510.

(15) Anderson, K. E.; Siepmann, J. I.; McMurry, P. H.; VandeVondele, J. *J. Am. Chem. Soc.* **2008**, *130*, 14144–14147.

(16) Hammerich, A. D.; Buch, V.; Mohamed, F. *Chem. Phys. Lett.* **2008**, *460*, 423–431.

(17) Kakizaki, A.; Motegi, H.; Yoshikawa, T.; Takayanagi, T.; Shiga, M.; Tachikawa, M. *THEOCHEM* **2009**, *901*, 1–8.

(18) Rode, B. M.; Hofer, T. S.; Randolf, B. R.; Schwenk, C. F.; Xenides, D.; Vchirawongkwin, V. *Theor. Chem. Acc.* **2006**, *115*, 77–85.

(19) Hofer, T. S.; Pribil, A. B.; Randolf, B. R.; Rode, B. M. Ab Initio Quantum Mechanical Charge Field Molecular Dynamics: A Nonparametrized First-Principle Approach to Liquids and Solutions. In *Combining Quantum Mechanics and Molecular Mechanics. Some Recent Progresses in QM/MM Methods*; Sabin, J. R., Brändas, E., Eds.; Academic Press: San Diego, 2010; Vol. 59, pp 213−246.

(20) Vchirawongkwin, V.; Rode, B. M.; Persson, I. *J. Phys. Chem. B* **2007**, *111*, 4150–4155.

(21) Vchirawongkwin, V.; Rode, B. M. *Chem. Phys. Lett.* **2007**, *443*, 4152–157.

(22) Pribil, A. B.; Vchirawongkwin, V.; Hofer, T. S.; Randolf, B. R. Structure and Dynamics of Composite Anions in Aqueous Solution. *Computation in Modern Science and Engineering, Proceedings of the International Conference on Computational Methods in Science and Engineering*; American Institute of Physics (AIP): New York, 2007; pp 921−923.

(23) Pribil, A. B.; Hofer, T. S.; Randolf, B. R.; Rode, B. M. *J. Comput. Chem.* **2008**, *29*, 2330–2334.

(24) Pribil, A. B.; Hofer, T. S.; Vchirawongkwin, V.; Randolf, B. R.; Rode, B. M. *Chem. Phys.* **2008**, *346*, 182–185.

(25) Vchirawongkwin, V.; Pribil, A. B.; Rode, B. M. *J. Comput. Chem.* **2010**, *31*, 249–257.

(26) Vchirawongkwin, V.; Kritayakornupong, C.; Ruangpornvisuti, V.; Rode, B. M. *THEOCHEM* **2009**, *913*, 236–239.

(27) Warshel, A.; Levitt, M. *J. Mol. Biol.* **1976**, *103*, 227–249.

(28) Field, M. J.; Bash, P. A.; Karplus, M. *J. Comput. Chem.* **1990**, *11*, 700–733.

(29) Gao, J. *J. Am. Chem. Soc.* **1993**, *115*, 2930–2935.

(30) Bakowise, D.; Thiel, W. *J. Phys. Chem.* **1996**, *100*, 10580–10594.

(31) Brooks, B. R.; Bruccoleri, R. E.; Olafson, B. D.; States, B. D.; Swaminathan, S.; Karplus, M. *J. Comput. Chem.* **1983**, *4*, 187–217.

(32) Berendsen, H. J. C.; Postma, J. P. M.; van Gunsteren, W. F.; DiNola, A.; Haak, J. R. *J. Chem. Phys.* **1984**, *81*, 3684–3690.

(33) Dunning, T. H., Jr.; Hay, P. J. In *Gaussian Basis Sets for Molecular Calculations*; Schaefer, H. F., III, Ed.; Plenum Press: New York, 1977; Vol. 3, Chapter 1, pp 1−27.

(34) Dunning, T. H., Jr. *J. Chem. Phys.* **1970**, *53*, 2823–2833.

(35) Stillinger, F. H.; Rahman, A. *J. Chem. Phys.* **1978**, *68*, 666–670.

(36) Bopp, P.; Janscó, G.; Heinzinger, K. *Chem. Phys. Lett.* **1983**, *98*, 129–133.

(37) Hofer, T. S.; Tran, H. T.; Schwenk, C. F.; Rode, B. M. *J. Comput. Chem.* **2004**, *25*, 211–217.

(38) Xenides, D.; Randolf, B. R.; Rode, B. M. *J. Chem. Phys.* **2005**, *122*, 174506.

(39) Lock, A. J.; Woutersen, S.; Bakker, H. J. *J. Phys. Chem. A* **2001**, *105*, 1238–1243.

(40) Bopp, P. *Chem. Phys.* **1986**, *106*, 205–212.

(41) Wang, X.-B.; Nicholas, J. B.; Wang, L.-S. *J. Phys. Chem. A* **2000**, *104*, 504–508.

(42) Frisch, M. J. et al. *Gaussian 03*, revision E.01; Gaussian, Inc.: Wallingford, CT, 2004.

(43) Godbout, N.; Salahub, D. R.; Andzelm, J.; Wimmer, E. *Can. J. Chem.* **1992**, *70*, 560–571.

(44) Kritayakornupong, C.; Vchirawongkwin, V.; Hofer, T. S.; Rode, B. M. *J. Phys. Chem. B* **2008**, *112*, 12032–12037.

(45) Kritayakornupong, C.; Vchirawongkwin, V.; Rode, B. M. *J. Comput. Chem.* **2010**, *31*, 1785–1792.

(46) Miller, F. A.; Carlson, G. L.; Bentley, F. F.; Jones, W. H. *Spectrochim. Acta* **1960**, *16*, 135–235.
(47) McQuarrie, D. A. *Statistical Mechanics*; Harper & Row: New York, 1976.
(48) *CRC Handbook of Chemistry and Physics*, 90th ed.; Lide, D. R., Ed.; CRC Press/Taylor and Francis: Boca Raton, FL, 2010.
(49) Sceats, M. G.; Rice, S. A. *J. Chem. Phys.* **1980**, *72*, 3236–3247.
(50) Mezei, M.; Beveridge, D. L. *J. Chem. Phys.* **1981**, *74*, 622–632.
(51) Luzar, A.; Chandler, D. *J. Chem. Phys.* **1993**, *98*, 8160–8173.
(52) Randolf, B. R.; Hofer, T. S.; Rode, B. M. Unpublished results.

JP105181N